

Urban photovoltaics reshape radiative–convective fluxes and cooling energy demand in cities

Hamza Nisar^{a,b,*}, Mattheos Santamouris^a, Christophe Menezo^b, Ansar Khan^c

^a School of Built Environment, University of New South Wales, Sydney, Australia

^b Building Energy Process Laboratory, Université Savoie Mont Blanc, Chambéry, France

^c Department of Geography, Lalbaba College, University of Calcutta, Kolkata, India

ARTICLE INFO

Keywords:

Rooftop photovoltaic panels
Building integration
Urban overheating
WRF simulations
Energy demand
Renewable energy

ABSTRACT

The rapid urbanization and transition to renewable energy are driving the adoption of rooftop photovoltaic solar panels (RPVSPs) to meet local energy demands. While their potential for clean energy generation is well-recognized, their broader impacts on urban microclimates, building energy consumption, and system performance remain poorly understood. This study examines the effects of RPVSPs on urban temperatures, energy balances, and cooling demand in Lyon, France, using high-resolution simulations with the weather research and forecasting (WRF) model. Results show that citywide installation of RPVSPs increase daytime temperatures by up to 0.72 °C, primarily because RPVSPs have a lower albedo compared to conventional rooftop surfaces, which leads to increased solar heat absorption and enhanced thermal convection between the panels and the underlying roof surfaces. This elevates the net sensible heat flux to the urban atmosphere during the daytime. Conversely, the nocturnal cooling of up to −0.42 °C results from radiative heat losses facilitated by the air gap and reduced thermal storage in RPVSPs covered roofs, enabling more efficient surface cooling after sunset. This dual thermal behavior reflects the RPVSPs influence on altering both the radiative and convective energy fluxes at the urban surface. While these effects may not exceed the cooling capacity of dedicated reflective or radiative cooling materials, the innovation in our study lies in quantifying the net thermal impact of real-world RPVSPs deployment at an urban scale. This dimension remains inadequately addressed in existing literature for temperate cities, especially in terms of balancing energy production with local microclimatic alterations. Additionally, RPVSPs reduce roof surface temperatures, cutting daytime air conditioning (AC) demand by nearly 5 %, particularly in areas with high roof-to-surface ratios. Immediate RPVSPs utilization achieved 100 % at 25 % RPVSPs coverage, offsetting 26.8 % of AC demand. At 60 % RPVSPs coverage, utilization dropped to 91.2 % with a 59.9 % AC offset, but storage enabled 100 % utilization and a 50.1 % offset. At full (100 % RPVSPs) coverage, immediate utilization declined to 64.3 % with a 73.0 % AC offset, while storage restored 100 % utilization, achieving an 85.9 % AC offset. High-resolution simulations reveal that RPVSPs simultaneously alter urban radiative–convective fluxes and cooling energy demand, highlighting their dual role in shaping city climate and energy resilience. Such strategies are vital for creating sustainable, energy-efficient urban environments that optimize renewable energy use while ensuring thermal comfort and resilience.

1. Introduction

The rapid growth of the rooftop photovoltaic solar panels (RPVSPs) industry is being driven by urgent shift towards low carbon energy solutions and the decreasing cost associated with RPVSPs technology [1]. The integration of building attached RPVSPs brings substantial social and economic benefits, such as produce energy where it is most needed, i.e. in cities, reducing the land use and associated costs, losses during electricity transport, and architectural benefits [2]. Scenarios have been

therefore developed to plan the massive integration of RPVSPs components in cities. This development is influencing the balance between the Earth's energy budget and land utilization patterns. Therefore, a comprehensive scientific assessment is essential to understand the consequences of extensive RPVSPs implementation in urban areas [3]. Lyon, with its temperate climate and diverse urban structure, offers a unique context to study RPVSPs impacts often overlooked in existing literature, such as dynamic energy flux interactions and socio-environmental trade-offs. Additionally, urban heterogeneity is

* Corresponding author.

<https://doi.org/10.1016/j.solener.2025.113928>

Received 1 May 2025; Received in revised form 17 July 2025; Accepted 25 August 2025

Available online 19 September 2025

0038-092X/© 2025 The Author(s). Published by Elsevier Ltd on behalf of International Solar Energy Society. This is an open access article under the CC BY license (<http://creativecommons.org/licenses/by/4.0/>).

frequently oversimplified, with local climate zones (LCZs) reduced to a few broad categories, limiting spatial accuracy in assessing RPVSPs impacts. Its participation in European sustainability initiatives makes it a relevant case for climate-responsive urban planning.

Foreseen future extensions of RPVSPs in urban environments offer a promising outlook in terms of low-carbon energy generation and cost efficiency [4]. However, these developments also present significant challenges. RPVSPs significantly influence the local environment and are, in turn, affected by it [5]. This includes their impact on ambient temperatures, changes in radiation, and the shadow cast by and on RPVSPs. While advancements in RPVSPs efficiency have been made, their impact on the urban environment and the rising urban heat island (UHI) effect remain areas of ongoing research. RPVSPs incorporated into buildings have a notable impact on albedo, reducing the reflectivity of roofs and contributing to the UHI effect [6]. A recent study on the environmental impact of RPVSPs revealed that they may significantly warm cities throughout the day. According to this research, this heating can also affect the performance of RPVSPs [5].

Numerous studies have employed regional climate modeling tools to assess the RPVSPs systems on urban environments. In the literature, many studies have demonstrated that RPVSPs contribute to reducing daytime temperatures. Ref. [7] conducted a study on urban areas of Los Angeles and investigated the impact of RPVSPs on the urban environment. He employed a simplified approach based on effective albedo and observed temperature reductions during the daytime by up to 0.2 °C and at night by up to 0.3 °C. The study assumed 30 % panel efficiencies and assumed dark roof surfaces (solar reflectance of 0.15). However, buildings in hotter climates often use higher reflectance roof coatings (solar reflectivity > 0.6), and even in moderate climates, rooftop solar reflectivity > 0.2. Setting albedo for all building rooftops to 0.15 was unrealistic.

Similar results were obtained by [8], they reported daytime cooling of up to 0.4 °C and nighttime cooling of up to 0.7 °C. This study assumed that panel temperature and ambient temperature were equal. However, RPVSPs panels have low thermal storage capacity, resulting in a small or negligible temperature difference between the lower and upper surfaces. RPVSPs surface temperatures frequently exceed 70 °C, particularly in hot locations. This assumption in the Masson study is inaccurate, leading to substantial errors in estimating convective heat transfer from RPVSPs to the surrounding air.

Another study [9] conducted in London demonstrated that integrating 100 % of RPVSPs systems can reduce daytime temperatures by up to 0.5 °C. In terms of UHI mitigation strategies, cool roofs have been shown to be highly effective. Another study conducted in China [10] revealed a cooling effect of 0.2 to 0.7 °C due to RPVSPs. The study proposes that RPVSPs can mitigate the UHI effect by reducing heat storage on roofs. However, this simplifies the complex heat transfer processes. While RPVSPs reduce the heat absorbed by roofs, they still convert a significant portion of solar energy into heat. Consequently, RPVSPs can reach temperatures of up to 70 °C, emitting this heat into the surrounding air, which can paradoxically increase temperatures in the vicinity. The reduction in heat storage on the roof (-47.32 Wm^{-2}) indicates a decrease in heat on the roof itself, but it fails to account for the heat transferred to the surrounding air. Therefore, while RPVSPs may reduce heat storage, they primarily redistribute heat, resulting in a net warming effect. Another study [11] employed the weather research and forecasting (WRF) model with datasets derived from the LCZ and gridded urban canopy parameters (UCPs) to simulate RPVSPs installations with 50 % (RPVSPs0.5) and 100 % (RPVSPs1.0) capacity in Guangzhou–Foshan. Under RPVSPs1.0, daytime cooling amounted to approximately 0.11 °C (LCZ-UCP) and 0.07 °C (gridded-UCP), while nighttime cooling ranged from 0.05 to 0.10 °C. In contrast, RPVSPs0.5 exhibited negligible or slight daytime warming, with values of -0.01 °C (LCZ-UCP) and $+0.03$ °C (gridded-UCP). Furthermore, RPVSPs0.5 induced modest nighttime cooling, with values ranging from 0.02 to 0.05 °C. Despite the reduction in sensible heat flux by 7.4 – 15.7 Wm^{-2} ,

RPVSPs still released stored heat during the day, resulting in partial warming. Nighttime cooling was attributed to limited roof heat storage and enhanced longwave emission. It is important to note that the results varied depending on the morphology dataset used, gridded-UCP predicted stronger cooling under RPVSPs0.5, while LCZ-UCP exhibited greater cooling under RPVSPs1.0. Key uncertainties associated with the study include uniform coverage assumptions, the omission of humidity and wind effects, and the differences in urban morphology representation.

In a study conducted by [12], the WRF model was integrated with the building effect parameterization (BEP) and building energy model (BEM) models to simulate extensive RPVSPs coverage during a heat-wave period spanning from August 21st to 27th, 2021, within the Chicago Metropolitan Area. The researchers findings indicated a significant reduction in daytime air temperatures by approximately 0.6 °C (11:00–17:00 LT), primarily attributed to the interception of solar radiation by RPVSPs panels. This process converts a portion of the solar energy into electrical energy, thereby mitigating the roof's sensible heat flux. Conversely, during the nighttime hours (00:00–06:00 LT), a modest warming of 0.1–0.2 °C was observed. The study assumed monocrystalline RPVSPs with 19 % conversion efficiency, 0.20 albedo, and 0.90 emissivity. This phenomenon can be attributed to a decrease in radiative heat loss from the roof and the continued convective release of residual panel heat under lower wind speeds. However, the study did not explicitly consider elevated RPVSPs panel temperatures, which often exceed 15–20 K above ambient during peak insolation, or the variability in panel emissivity. These factors would increase sensible and longwave heat release, consequently altering both the magnitude of daytime cooling and nocturnal warming.

A separate study in China [13] found that daytime cooling can range from 0.1 to 0.5 °C, while nighttime cooling can range from 0.2 to 0.4 °C, depending on the efficiency of RPVSPs. In contrast, while [14] demonstrated that Singapore can experience a daytime temperature drop of up to 1 °C, the study's conclusions regarding the cooling effect of RPVSPs panels are questionable. The study suggests that RPVSPs reduce near-surface air temperature by mitigating roof heat storage and maintaining lower panel temperatures through partial energy conversion. Furthermore, it asserts that, based on Stefan-Boltzmann's law, similar emissivity but lower RPVSPs temperatures result in reduced longwave radiation to the surrounding air. However, this assumption is erroneous. RPVSPs absorb approximately 80–85 % of solar radiation and typically attain high surface temperatures often surpassing standard roofing materials. Consequently, they emit more thermal radiation, not less. The assertion of reduced emissions is contingent upon the inaccurate presumption that RPVSPs do not experience substantial heating. Consequently, the reported cooling of ambient temperature is likely a consequence of oversimplified thermal modeling rather than a genuine physical phenomenon. Most of the models considered only the radiative properties of RPVSPs. However, RPVSPs also influence surface-atmosphere interactions and processes that were poorly understood and neglected in their RPVSPs land surface modeling, such as surface roughness and convective heat transfer [15].

Numerous other studies conducted using numerical simulations and examining actual or empirical data yielded conflicting results compared to the work mentioned above. A study highlighted that the temperature of local air can be elevated due to the installation of RPVSPs, primarily because of their low energy conversion efficiency [16]. An observational study conducted in southern Arizona revealed a significant increase of 1.3 °C in the daily average air temperature as a result of the presence of RPVSPs arrays [15]. However, the impact of RPVSPs installations on local climate varies across different climatic regions and RPVSPs characteristics [5]. In a numerical study conducted on Kolkata, India, it was found that RPVSPs installed in urban environments can cause a temperature increase of 1.4 °C during the day and a decrease of 2.3 °C at night [17]. A comparable study conducted in Sydney yielded similar findings, with temperature rising by up to 1.5 °C during the day and

falling by up to 2.7 °C at night [18]. These studies revealed that the installation of RPVSPs on rooftops has a substantial impact on sensible heat flux and convection, leading to an increase in daytime temperatures. A study has shown that the thermal impact of RPVSPs is more pronounced in low-rise buildings due to their lower thermal inertia and greater influence on near-surface air temperature [19]. In such configurations, RPVSPs can increase daytime temperatures by up to 1.5 °C, while at night, as their thermal mass is low reduced heat storage can lead to cooler conditions up to 0.5 °C lower. This effect diminishes with increasing building height, where rooftops have less influence on the surrounding air temperature. A comprehensive study was conducted to assess the thermal impact of RPVSPs [20]. The study revealed that the daytime ceiling temperature beneath a RPVSPs array was up to 2.5 °C cooler compared to an unprotected roof. Heat flux modeling indicated a substantial reduction in daytime roof heat flux under the RPVSPs array. At night, the conditions reversed, and the ceiling under the RPVSPs arrays was warmer than for the exposed roof, indicating the insulating properties of RPVSPs. Across the reviewed WRF-based studies including Chicago [12], Chaoyang [13], Singapore [14], Kolkata [17], and Guangzhou [11], RPVSPs were uniformly parameterized with albedo values ranging from 0.10 to 0.20, emissivity's ranging from 0.79 to 0.95, conversion efficiencies ranging from 0.10 to 0.30 (typically approximately 0.19), temperature coefficients ranging from -0.005 to -0.008 °C $^{-1}$, equivalent heat capacities of 5.72 MJ m $^{-2}$ K $^{-1}$, thermal conductivities near 1 W m $^{-1}$ K $^{-1}$, coverage fractions ranging from 25 % to 100 %, mounting heights ranging from 0.3 to 0.8 m, and panel thicknesses of approximately 6.5 mm.

In light of the diverse and occasionally conflicting findings in the literature, it is evident that the environmental impacts of RPVSPs panels in urban settings are multifaceted and highly local context dependent. Therefore, this study aims to provide a comprehensive analysis of the effects of RPVSPs on the urban environment, focusing specifically on diurnal variations in temperature, surface and atmospheric heat transfers, and energy generation. Additionally, we investigate how the presence of RPVSPs influences urban energy consumption patterns particularly the potential shift in cooling demands due to changes in rooftop heat fluxes and indoor temperatures. To achieve this, the study employed the WRF model coupled with an urban canopy and land surface model to simulate the dynamic interactions between RPVSPs installations and the urban climate. Using a realistic urban setup for Lyon, this work seeks to enhance the understanding of RPVSPs integration impacts on both the thermal and energy dynamics of cities across day and night cycles.

2. Methodology

2.1. Model domain

Lyon, the third-largest city in France, is located in southeastern Auvergne-Rhône-Alpes. Situated at the confluence of the Rhône and Saône Rivers, it's about 470 km southeast of Paris and 320 km north of Marseille. Lyon experiences a temperate oceanic climate with an average annual temperature of 12 °C, fluctuating from 3 °C in January to 20 °C in July. The average annual global horizontal irradiance is 1200 kWh m $^{-2}$ yr $^{-1}$, varying from 2.75 kWh m $^{-2}$ day $^{-1}$ in January to 5.75 kWh m $^{-2}$ day $^{-1}$ in July. Relative humidity averages 75 %, and 10 m wind speeds range from 1.5 m s $^{-1}$ in summer to 3.0 m s $^{-1}$ in winter. Annual precipitation is about 820 mm.

Lyon experiences the UHI, leading to elevated nighttime temperatures, especially in densely urbanized areas. To address this, a nested domain strategy with three domains was employed. The outermost domain (d01) had a resolution of 3.5 km, followed by the second domain (d02) with a refined resolution of approximately 1.17 km (1/3 nesting ratio). The innermost domain (d03) had the highest resolution, around 390 m, enabling detailed analysis of the city's specific meteorological conditions. The grid dimensions for the domains were 150×150 for

d01, 130×130 for d02, and 100×100 for d03 as shown in Fig. 1.

This study used a hybrid 100-m global land cover dataset developed by [21] to represent urban morphology in WRF simulations. The dataset integrates copernicus global land cover (CGLC) and LCZ classifications, providing a standardized classification of land cover, including vegetation and urban categories. This ensures consistent representation of surface characteristics, as shown in Fig. 1. The dataset is used to parameterize land surface properties and urban energy balance dynamics, enabling a comprehensive evaluation of RPVSPs' interaction with the urban environment.

2.2. Model setup

The WRF model version 4.5.2 assessed the impact of RPVSPs on urban temperatures and surface energy fluxes, focusing on Lyon, France. The study used the WRF/BEP + BEM system to simulate urban microclimates and RPVSPs effects (see Supplementary Fig. S1 for schematic). This integrated approach evaluated urban-atmosphere interactions, including heat exchange, momentum transfer, humidity flux, and turbulent kinetic energy. The model also incorporated building-level dynamics, such as heat conduction, natural ventilation, indoor radiative exchange, internal heat gains, and air conditioning (AC) energy consumption. Indoor thermal dynamics were simulated BEM component, which models each zone as a well-mixed control volume with coupled energy and moisture balances in Supplementary Section S1; [22]. This configuration enables dynamic coupling between indoor environmental conditions and the urban microclimate. The initial and lateral boundary conditions were established using high-resolution european centre for medium-range weather forecasts (ECMWF) data [23,24]. Key physics parameterization schemes are summarized in Table 1. The simulation ran from August 14, 2023, at 00:00 LT to August 20, 2023, at 00:00 LT, with a 10,800-second (3-hour) integration time step for meteorological boundary condition updates. The comprehensive modeling framework and workflow for the WRF simulation setup are detailed in Fig. S2.

2.3. Rooftop photovoltaic solar panels parameterization

The parameterization of RPVSPs within the WRF/BEP + BEM system, developed by [19], models RPVSPs as parallel, detached single-layer arrays. The temperature time derivative is calculated by considering various energy fluxes, including net shortwave radiation, incoming longwave radiation, and longwave radiation exchange between the RPVSPs and the roof. The model consists of three layers: monocrystalline silicon, polyester trilaminate, and glass, with material properties from [32]. Notably, energy production efficiency decreases when temperatures exceed 25 °C. This method differs from previous studies [8,7] by directly solving the energy balance to calculate RPVSPs temperature, providing a more accurate representation of all factors. The resulting heat flux is updated and passed to the multilayer urban scheme. The parameterization scheme is detailed in the literature, with the time derivative of the RPVSPs temperature represented by the equation [19].

$$\frac{dT_{RPVSPs}}{dt} = \frac{1}{C_p} (R_n - E_{RPVSPs} - Q_h) \quad (1)$$

where R_n denotes net radiation, E_{RPVSPs} is energy production and Q_h is total heat flux.

$$\frac{dT_{RPVSPs}}{dt} = \frac{1}{C_p} \left(R_{sw,in} + R_{lw,in} - R_{lw,out,RPVSPs} + R_{lw,exchange} - E_{RPVSPs} - Q_{up} - Q_{down} + R_{lw,down} \right) \quad (2)$$

The area heat capacity of the composite laminate, C_p , is calculated as 5.72 MJ K $^{-1}$ m $^{-2}$ based on the composition of the RPVSPs, glass face,

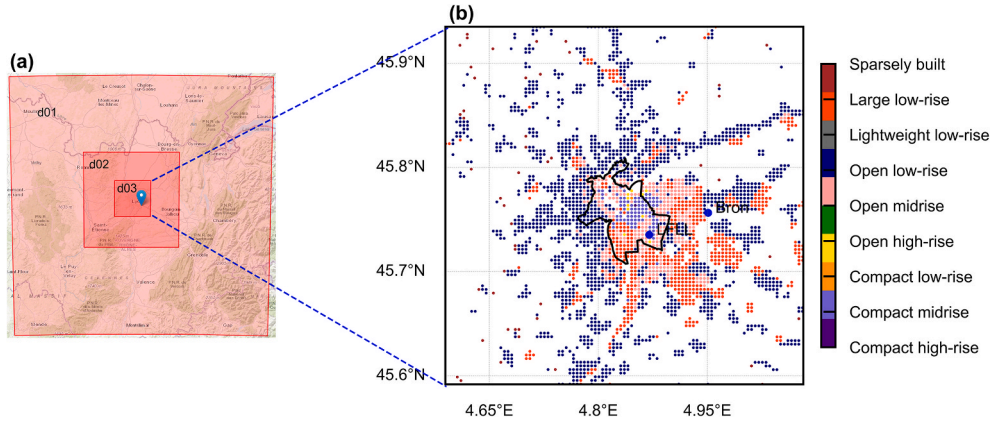


Fig. 1. WRF model setup and urban land classification over Lyon, France. Panel (a) shows the nested domain configuration used in the WRF simulations, with the innermost domain (d03) centered over the city of Lyon for high-resolution urban analysis. Panel (b) presents the CGLC urban classification map used for surface characterization within the simulation domain.

Table 1

Physics parameterization schemes used in the WRF model

Physics process	Scheme
Multi-layer urban canopy model	WRF/BEP + BEM [22]
Microphysics	WRF single-moment six-class [25]
Land surface model	Noah-MP [26]
Planetary boundary layer	Bougeault-Lacarrere [27]
Turbulence	Janjić TKE scheme [28]
Shortwave radiation	Dudhia scheme [29]
Longwave radiation	Rapid radiative transfer model [30]
Cumulus parameterization	Kain-Fritsch scheme [31]

Table 2

Properties of RPVSPs panel

Properties	Value
Albedo	0.11
Upper face emissivity	0.79
Downward face emissivity	0.95
Conversion efficiency	0.19
Cell depth	6.55 mm
Temperature coefficient	0.0045 °C ⁻¹

polyester trilaminate, and monocrystalline-silicon cell. The total depth of these layers is 6.5 mm. Specific values of heat capacity, thickness, and density for each layer are provided in [33]. Net short-wave gain on the upward face is $R_{sw,inc} = (1 - \alpha_{RPVSPs}) \times SW_{inc}$ with $\alpha_{RPVSPs} = 0.11$. Incoming long-wave radiation is $R_{lw,inc} = \epsilon_{RPVSPs}^U LW_{sky,down}$ using an upward emissivity $\epsilon_{RPVSPs}^U = 0.79$, while the panel's own emission is $R_{lw,out,RPVSPs} = \epsilon_{RPVSPs}^U \sigma T_{RPVSPs}^4$. Long-wave exchange with the roof beneath is:

$$R_{lw,exchange} = VF \frac{1}{\frac{1 - \epsilon_{RPVSPs}^D}{\epsilon_{RPVSPs}^D} + \frac{1 - \epsilon_{roof}}{\epsilon_{roof}}} \sigma (T_{RPVSPs}^4 - T_{roof}^4) \quad (3)$$

with view factor $VF = 0.06$ for a $10 \text{ m} \times 10 \text{ m}$ array at 0.3 m clearance and a downward emissivity $\epsilon_{RPVSPs}^D = 0.95$. Useful electrical production is parameterized as

$$E_{RPVSPs} = \eta_{RPVSPs} SW_{inc} \min[1.1 - 0.005(T_{RPVSPs} - 298.15)] \quad (4)$$

where $\eta_{RPVSPs} = 0.19$ the bracketed factor accounts for the documented efficiency loss above 25°C . Sensible heat exchange with the ambient air and the shaded roof is $Q_{up} = h_{up}(T_{RPVSPs} - T_{air})$ and $Q_{down} = h_{down}(T_{RPVSPs} - T_{roof})$ respectively; the transfer coefficients h_{up} and h_{down} follow the EnergyPlus empirical formulation $h = \sqrt{h_c^2 + a|V|^2}$ validated by [34]. Finally, the isotropic short-wave and long-wave flux incident on the panel's underside is $R_{lw,down} = (1 - VF) [(1 - \alpha_{RPVSPs}) SW_{diff} + LW_{sky}]$ the same amount being received by the underlying roof surface. Together, these terms close the surface energy balance driving the time evolution of T_{RPVSPs} in the WRF-BEP + BEM simulations. Table 2 represents the properties of RPVSPs used in WRF simulation:

2.4. Simulation scenarios for rooftop photovoltaic solar panels

Three primary simulation scenarios assessed the impact of RPVSPs

systems on urban temperature dynamics. The baseline Scenario (No RPVSPs) represents the current urban land-use configuration in Lyon, excluding RPVSPs, with a rooftop albedo of 0.2, based on studies in the city [35,36]. The RPVSPs scenarios introduce rooftop RPVSPs panels at varying coverage levels (25 %, 60 %, and 100 %). The data analysis focused on near-surface temperature variations, energy fluxes, and building energy dynamics. It compared the base scenario with the RPVSPs scenarios to quantify the effect of RPVSPs systems on urban temperatures. Changes in roof heat flux, sensible heat flux due to shading, and reflective properties were also examined. Building cooling energy load was assessed to understand the impact of solar shading and heat transfer from RPVSPs on reducing cooling energy consumption. RPVSPs energy production was calculated for each coverage scenario based on solar radiation and panel efficiency to determine the potential for RPVSPs systems to meet the city's electricity demand. This approach, implemented in WRF v4.5.2, provides a comprehensive framework for evaluating the effects of varying RPVSPs coverage on urban thermal dynamics, energy fluxes, and energy consumption, contributing to sustainable urban planning and climate mitigation strategies, especially in integrating renewable energy technologies in urban areas.

3. Results and discussions

3.1. Model validation and evaluation

To assess the WRF/BEP + BEM system's efficacy, hourly simulated 2-m ambient air temperatures were compared with local observations in urban grid cells within the innermost domain for the control scenario. Measurements from two meteorological stations in Lyon-Bron and Saint-Exupéry (LFLL) were used from August 16 to 20, 2023.

Statistical metrics, root mean square error (RMSE), bias, R, and R^2 were calculated to evaluate the model's accuracy. At the first location, the WRF model had an RMSE of 2.06, a bias of -0.90 , an R of 0.94, and an R^2 of 0.88, indicating a slight underestimation. However, the high correlation and R^2 values suggest strong agreement. At the second

location, the RMSE was 1.85, the bias was -0.10 , the R was 0.95, and the R^2 was 0.90, as shown in Fig. 2. These results indicate high accuracy and strong agreement with observed temperatures at both locations. Similar validation results have been observed in numerous studies [10,17,18], supporting the WRF model's efficacy in replicating local meteorological conditions and its application in UHI studies.

3.2. Impact on near-surface temperature during daytime

The study examined the effects of large-scale RPVSPs deployment on near-surface air temperature (T_2) using the WRF model, with RPVSPs coverage levels at 25 %, 60 %, and 100 %. At 11:30 LT, the 2-meter air temperature increased by 0.20°C , 0.48°C , and 0.72°C for the respective coverage scenarios compared to the baseline without RPVSPs, as shown in Fig. 3. A diurnal analysis of average temperature variation across urban areas is presented in Fig. 4. For 25 % RPVSPs coverage, temperature differences ranged from -0.06°C at 5:30 LT to 0.06°C at 11:00 LT. For 60 % coverage, they ranged from -0.10°C at 20:30 LT to 0.18°C at 10:00 LT, and for 100 % coverage, from -0.18°C at 20:30 LT to 0.28°C at 11:00 LT. The highest temperature rise was observed in zones with compact mid-rise buildings, while the lowest was in zones with low-rise open buildings. The temperature increase in RPVSPs regions is mainly due to changes in the surface energy balance. RPVSPs panels, with low albedo as shown in Fig. 5, absorb more solar radiation than conventional rooftops, leading to higher surface temperatures and increased heat transfer to the atmosphere.

Direct sunlight exposure can cause RPVSPs to reach temperatures up to 70°C , as illustrated in Fig. 6, contributing to air warming. Similar findings were reported in another study [17]. The monocrystalline RPVSPs under study have low thermal inertia due to their 6.55 mm thickness, allowing rapid heating and heat release, leading to noticeable local air temperature increases, especially around 10:00 LT [17,19].

RPVSPs rapidly transfer heat to the air, intensifying heat exchange from rooftops. This effect raises air temperatures, particularly in the morning when heat absorption is highest. RPVSPs installation leads to higher temperatures than control scenarios due to greater sensible heat generation by the panels and roof. The low albedo of RPVSPs also causes localized warming through enhanced thermal convection.

Additionally, RPVSPs are elevated 0.3 m above the roof, creating a ventilation gap that promotes convective airflow. This setup results in two heat surfaces: one exposed to solar radiation and the underside above the roof, intensifying convective heat transfer and amplifying temperature increases as shown in Fig. 7. This contributes to localized warming and alters the urban microclimate. While 15–20 % of absorbed solar energy is converted into electricity, the remainder is released as heat, enhancing near-surface atmospheric warming.

RPVSPs panels influence urban temperatures by altering the surface energy balance. Fig. 8 shows atmospheric temperature up to 1 km at 10:00 LT with respect to a base case of 0 % RPVSPs installation. With 100 % RPVSPs coverage, the 2 m air temperature increased by up to 0.25°C , with warming effects extending vertically up to 0.6 km in urbanized regions. A cooling zone of up to 0.27°C was observed between 0.6–0.9 km due to altered vertical heat transport and convective processes. For 60 % RPVSPs coverage, the warming effect was less pronounced, with a maximum temperature increase of 0.176°C . Similar cooling trends were detected above 0.7 km. At 25 % coverage, surface warming was minimal, and enhanced cooling occurred above 0.8 km, likely due to reduced surface heat flux and weaker convective activity. These findings demonstrate that increased RPVSPs coverage leads to enhanced surface warming and significant modifications in vertical heat redistribution and convective processes.

To evaluate the seasonal reliability of RPVSPs induced temperature effects, additional simulations were conducted for a representative spring period from March 26–31, 2023, using the same WRF/BEP +

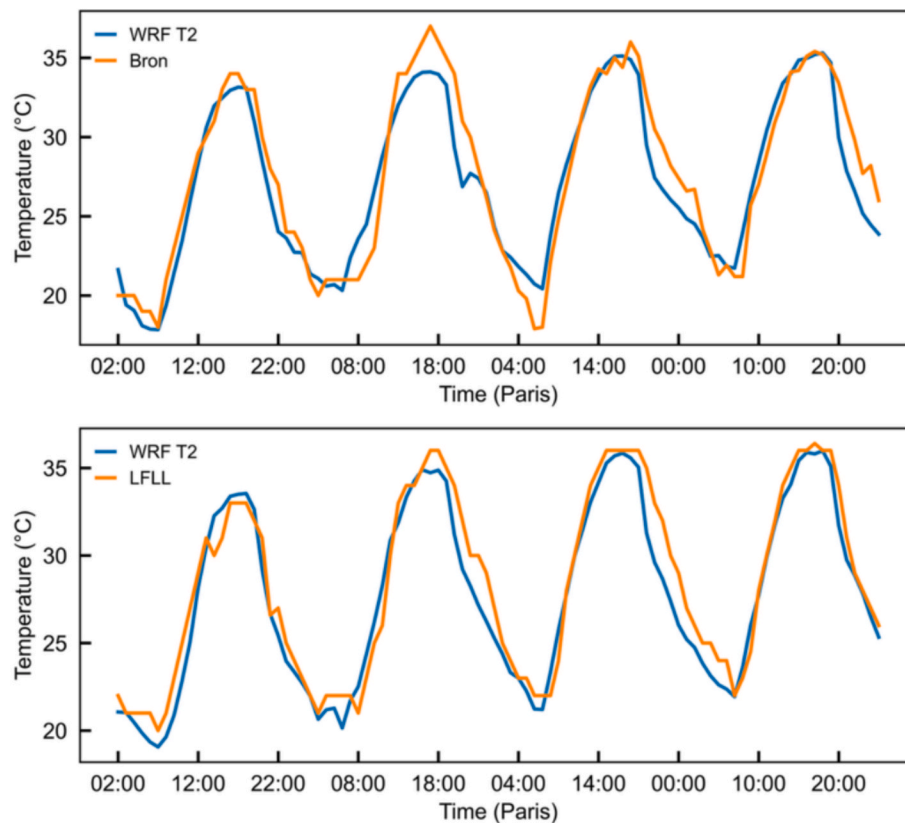


Fig. 2. Model validation through comparison with observed weather station data at multiple locations across Lyon, demonstrating the accuracy of simulated temperature and meteorological parameters.

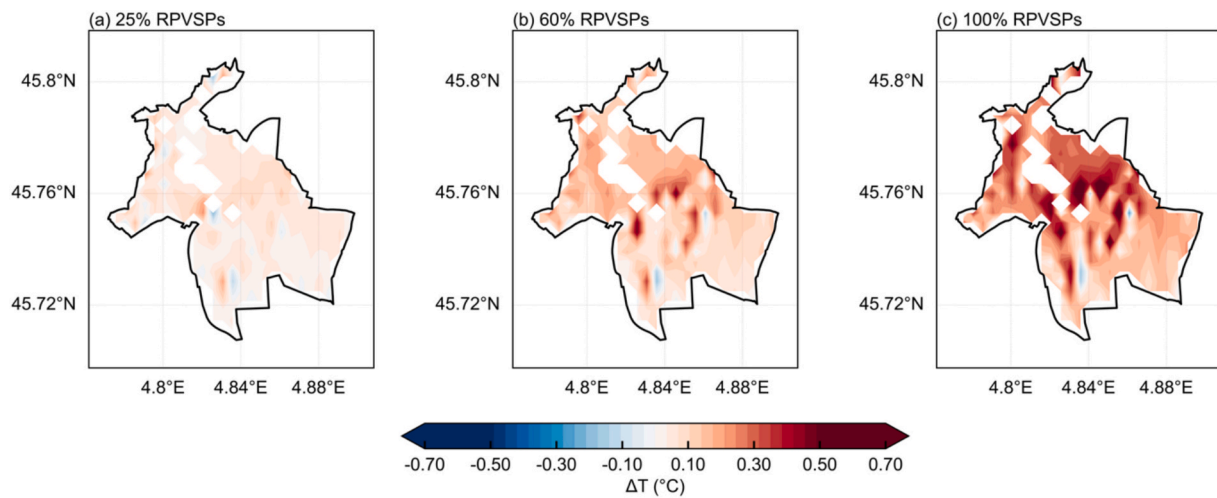


Fig. 3. Spatial distribution of daytime (11:30 LT) 2-m air temperature differences between RPVSPs deployment scenarios 25 %, 60 %, and 100 % and the baseline scenario (0 % RPVSPs) over the urban area of Lyon. The differences are calculated as RPVSPs scenario minus baseline (0 % RPVSPs), illustrating the impact of increased RPVSPs coverage on urban air temperature. The urban extent of Lyon is outlined in black. Panels represent: (a) 25 % RPVSPs, (b) 60 % RPVSPs, and (c) 100 % RPVSPs.

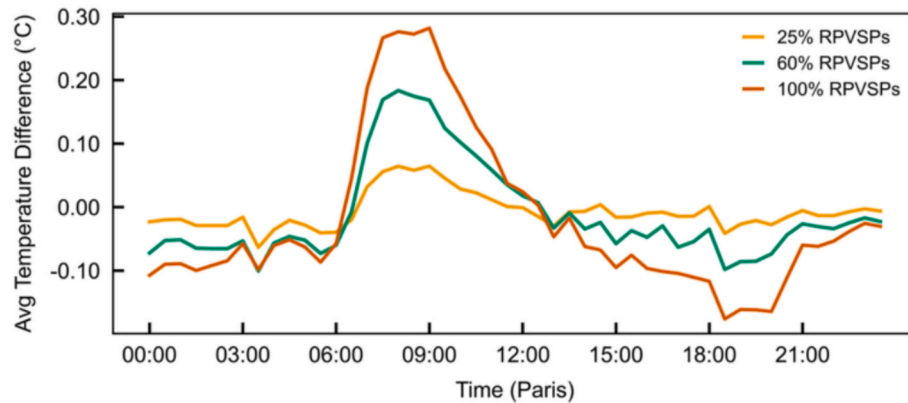


Fig. 4. Average daytime 2-m air temperature difference in Lyon for 25 %, 60 %, and 100 % RPVSPs deployment scenarios compared to the baseline (0 % RPVSPs).

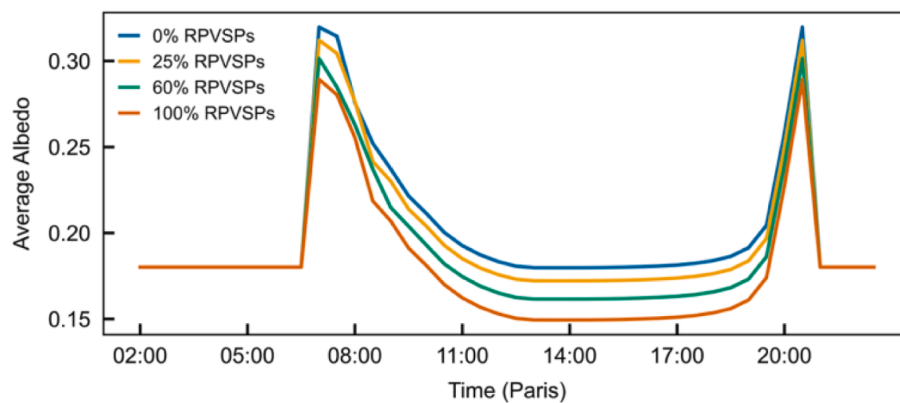


Fig. 5. Time Series of surface albedo for different RPVSPs deployment scenarios (25 %, 60 %, and 100 %).

BEM configuration. [Supplementary Fig. S3](#) illustrates that the spatial distribution of 2m air temperature changes at 25 %, 60 %, and 100 % RPVSPs coverage levels shows localized surface warming patterns over urban areas, similar in magnitude and spatial extent to those observed in the summer simulation. [Supplementary Fig. S4](#) further demonstrates the diurnal temperature differences, confirming that the temporal trends in

RPVSPs induced warming persist under moderate seasonal conditions. These findings confirm the consistency of modeled thermal impacts across different meteorological conditions and enhance the robustness of the results.

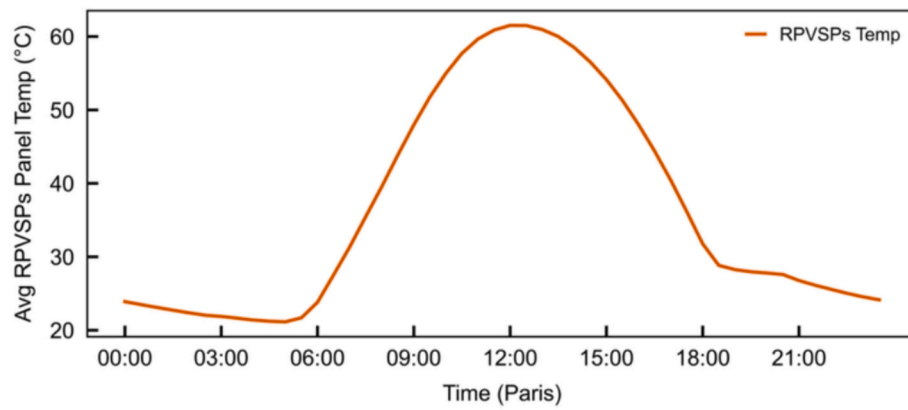


Fig. 6. RPVSPs temperature at hourly scale.

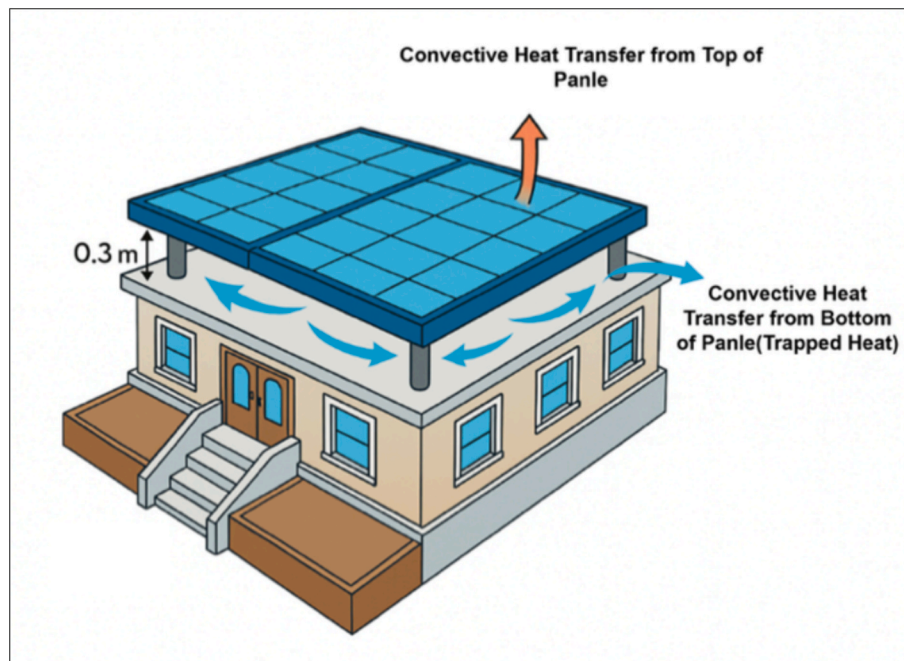


Fig. 7. Intensified convection process due to heating of RPVSPs.

3.3. Impact on near-surface temperature during nighttime

At 20:00 LT, a consistent temperature decrease was observed across all RPVSPs coverage levels. The maximum temperature drops were 0.27 °C for 25 % coverage, 0.30 °C for 60 %, and 0.42 °C for 100 %, as illustrated in Fig. 9. During nighttime, RPVSPs primarily function as efficient radiative surfaces despite their low thermal inertia. Their sky-facing orientation and high emissivity facilitate efficient emission of longwave radiation to the cold sky, resulting in net radiative energy loss. Under clear-sky conditions, this enables rapid cooling, often to temperatures below ambient air, leading to a slight reduction in near-surface air temperatures. While RPVSPs introduce thermal resistance, their elevated geometry and emissive properties prioritize sky-facing radiative cooling over ground-level conductive release. Consequently, the nocturnal cooling observed in simulations stems from dynamic radiative exchange and modified convective regimes, particularly under calm, clear conditions.

The nighttime cooling effect in urban areas with RPVSPs arises from a combination of radiative and enhanced convective cooling of the shaded rooftop surface beneath the panels. Although RPVSPs can reduce direct nighttime radiative heat loss from the roof, enhanced convective

cooling within the panel-roof gap mitigates this, leading to reduced urban surface temperatures. Unlike conventional building surfaces that retain heat more effectively, RPVSPs exhibit lower heat retention, facilitating quicker cooling. This interplay contributes to a net temperature decrease in the urban environment during the evening.

Literature reports cooling effects ranging from 0.2 °C to 1.0 °C, as shown in Fig. 10, primarily due to attributed to shading and reduced sensible heat flux. For instance, a study by [37] documented a 0.2–0.4 °C reduction in Phoenix–Tucson with 100 % RPVSPs coverage. Masson et al. [8] observed over 0.2 K of daytime cooling in Parisian suburbs due to the high conversion efficiency and emissivity of thermal RPVSPs. Another study [38] showed up to 1.2 °C of cooling in Singapore under full RPVSPs deployment in low-rise, high-density areas, influenced by high emissivity and sea-breeze advection. In contrast, the current study indicates that RPVSPs can increase city 2m air temperature by up to 0.7 °C due to panel heating and convective heat flux. Daytime warming has been widely reported, with increases up to 1.5 °C in high-density urban settings with low-albedo RPVSPs materials and extensive panel coverage [39,17,18,40,19]. Hirano and Yoshida [39] found a 0.1–0.2 °C daytime air temperature increase in Japanese office/residential districts due to low RPVSPs albedo. A study by [18] demonstrated that 100 % RPVSPs

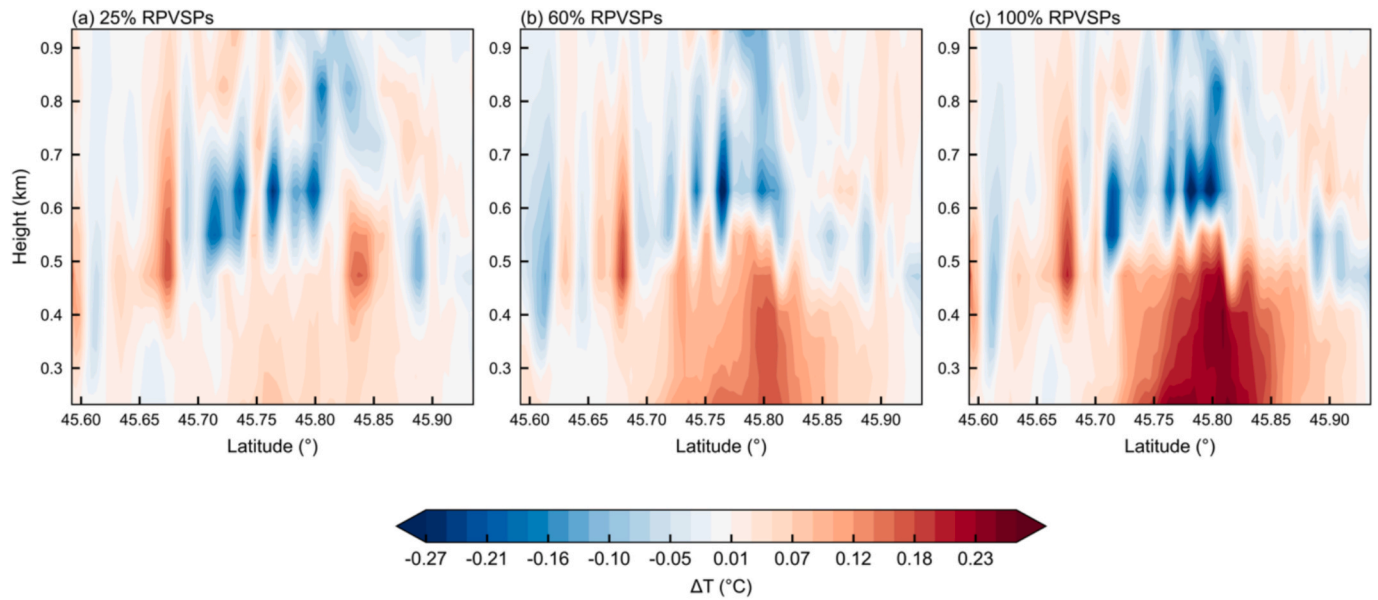


Fig. 8. Cross-sectional view of atmospheric temperature differences for 25 %, 60 %, and 100 % RPVSPs coverage compared to the base (0 % RPVSPs) scenario.

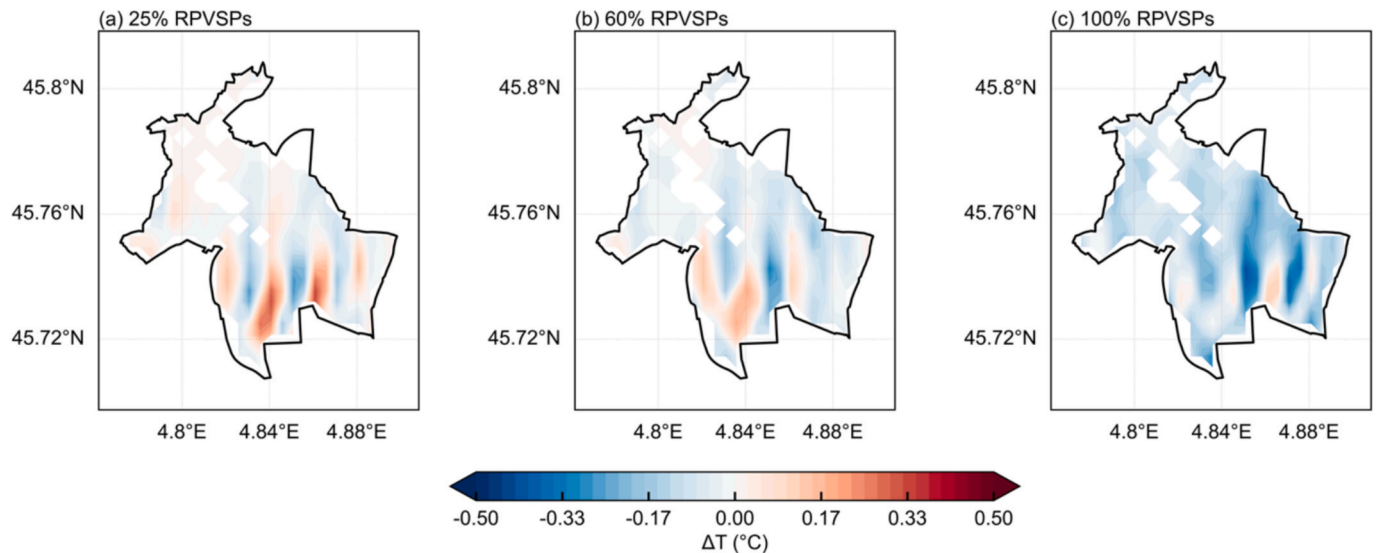


Fig. 9. Spatial distribution of nighttime (20:00 LT) 2-m air temperature differences between rooftop photovoltaic (RPVSPs) deployment scenarios 25 %, 60 %, and 100 % and the baseline scenario (0 % RPVSPs) over the urban area of Lyon. The differences are calculated as RPVSPs scenario minus baseline (0 % RPVSPs), illustrating the impact of increased RPVSPs coverage on urban air temperature. The urban extent of Lyon is outlined in black. Panels represent: (a) 25 % RPVSPs, (b) 60 % RPVSPs, and (c) 100 % RPVSPs.

coverage in Sydney resulted in up to 1.5 °C daytime warming, as panel-induced roof-surface temperatures reached 55–65 °C, enhancing sensible heat flux despite electrical generation. Our WRF simulations corroborate this trend, indicating 2 m air temperature increases of 0.20 °C, 0.48 °C, and 0.72 °C at 11:30 am under 25 %, 60 %, and 100 % RPVSPs coverage, respectively. Pokhrel et al. [40] observed a 0.6 °C temperature increase in mid-rise sectors with 75 % RPVSPs coverage due to enhanced sensible heat retention from constrained urban-canyon ventilation. Our simulations further demonstrate that compact mid-rise zones experience the most significant warming, primarily due to increased sensible heat flux from RPVSPs in poorly ventilated canyon geometries.

Nighttime impacts were more consistent, with most studies reporting a cooling effect of 0.3 °C to 0.8 °C as shown in Fig. 10. This is attributed to the low thermal inertia of RPVSPs panels, facilitating rapid heat

dissipation after sunset. Previous studies [37,38] reported nocturnal cooling of 0.4–0.8 °C in Phoenix–Tucson and Singapore, respectively, attributed to rapid heat loss. A study by [8] noted 0.3 K of nighttime cooling in Parisian suburbs, linked to reduced daytime heat storage and increased rooftop panel longwave emission. Another study [11] reported 0.2–0.4 °C of nocturnal cooling in Chaoyang under 100 % RPVSPs coverage, with occasional slight warming at lower coverage (02:00–06:00 LT) due to residual insulation. The current study observed minor nighttime cooling across all deployment levels, with the most significant decrease under 100 % RPVSPs coverage. Although smaller in magnitude than some reported values, the consistent direction and trend confirm the role of RPVSPs surfaces in reducing residual nighttime urban heat.

Our findings align with the study by [17], who observed similar trade-offs between rooftop cooling and daytime air warming in Kolkata,

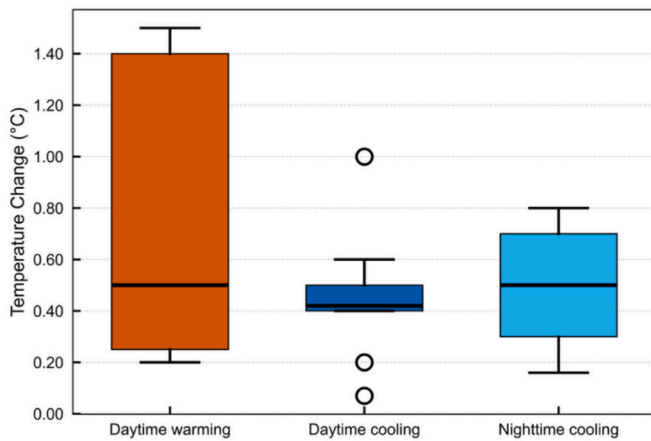


Fig. 10. Boxplot showing temperature changes associated with RPVSPs installations reported across different studies. “daytime warming” refers to observed increases in 2-m air temperature, while “daytime cooling” and “nighttime cooling” represent temperature reductions. The interquartile range, median, and outliers are illustrated, highlighting the variability of RPVSPs impacts under different conditions. (Data shown in [supplementary Table 2](#)).

and with studies conducted in Sydney, Austin, Athens, and Brussels, which demonstrated comparable shifts in surface energy balance. This study stands out by integrating high-resolution surface parameters and focusing on extreme summer conditions within a temperate-oceanic climate zone. This approach enables the capture of nuanced RPVSPs effects, including nighttime radiative suppression.

[Supplementary Fig. S5](#) shows the spatial distribution of 2 m air temperature differences at 20:00 LT for 25 %, 60 %, and 100 % RPVSPs coverage during spring (March 26–31, 2023), relative to the 0 % baseline. The observed evening cooling patterns mirror those from summer ([Fig. 9](#)), reinforcing consistency of RPVSPs induced thermal responses across seasons. This comparative framework validates our findings and enhances generalizability, providing insights into urban morphology, solar installations, and local climate dynamics. LCZ approach, employed to represent urban morphology, facilitates spatially explicit and typology-sensitive assessments of thermal impacts. Unlike earlier WRF studies, the LCZ framework offers a finer resolution of urban form, surface materials, and land cover effects, thereby enhancing the accuracy of localized temperature effects of RPVSPs as depicted in [Figs. 3 and 9](#). Detailed LCZ implementation and classifications are provided in [Table S1](#).

3.4. Impact on surface energy budget

The city-wide deployment of RPVSPs significantly impacted the

sensible heat flux (Q_{sensible}) from urban surfaces. At 10:30 LT, the average Q_{sensible} was 112.3 Wm^{-2} for 25 % RPVSPs coverage, 116.5 Wm^{-2} for 60 % coverage, and 121.1 Wm^{-2} for 100 % coverage, as shown in [Fig. 11](#). After 12:00 LT, Q_{sensible} decreased due to reduced anthropogenic heat emissions, particularly from AC units, as cooling demand declined, leading to a decrease in waste heat release into the environment [10].

Solar shading from RPVSPs blocks direct solar radiation, reducing roof heat flux. Although longwave and diffused radiation partially offset this, the decreased direct solar heating of the roof results in a lower overall roof heat flux [9,41]. At 12:00 LT, the roof heat flux for the base case (0 % RPVSPs) ranged from -179.87 Wm^{-2} to -464.75 Wm^{-2} , with an average of -257.70 Wm^{-2} , indicating heat transfer into the building. With 25 % RPVSPs coverage, the flux decreases, with a minimum of -172.41 Wm^{-2} , a maximum of -449.08 Wm^{-2} , and an average of -245.59 Wm^{-2} , indicating reduced heat transfer. For 60 % and 100 % RPVSPs coverage, the flux remains negative, with minimum and maximum values of -159.61 Wm^{-2} and -414.10 Wm^{-2} (average of -227.59 Wm^{-2}) for 60 % RPVSPs, and -139.23 Wm^{-2} and -387.83 Wm^{-2} (average of -202.38 Wm^{-2}) for 100 % RPVSPs, indicating continued heat transfer but at a lower rate. Shading effects reduce the downward heat flux, decreasing the thermal load on buildings and lowering AC demand, which leads to reduced anthropogenic heat emissions, particularly from buildings, as shown in [Fig. 12](#).

RPVSPs influence net radiation diurnally due to changes in surface energy absorption and emission. During the day, net radiation increases with higher RPVSPs coverage due to lower panel albedo, enhanced solar radiation absorption, and elevated surface temperatures. For 100 % RPVSPs coverage, net radiation rises by 76.5 Wm^{-2} , for 60 % coverage by 41.1 Wm^{-2} , and for 25 % coverage by 15.3 Wm^{-2} . This demonstrates a direct correlation between RPVSPs coverage and energy retention, as illustrated in [Fig. 13](#). Conversely, at night, net radiation decreases with higher RPVSPs coverage. RPVSPs high emissivity, especially in the thermal infrared range, efficiently emits longwave radiation to the clear night sky, causing radiative cooling and a decrease in net radiation. Convective heat loss and low thermal mass further enhance this cooling effect. These characteristics limit heat retention and enable efficient nighttime cooling. Consequently, net radiation decreases by 21.4 Wm^{-2} for 100 % RPVSPs, 11.3 Wm^{-2} for 60 % RPVSPs, and 5.6 Wm^{-2} for 25 % RPVSPs during night. This suggests that while RPVSPs panels enhance daytime heat absorption, they also diminish nighttime radiative cooling, impacting urban thermal dynamics and heat retention.

RPVSPs effectively reduce roof temperatures but increase daytime ambient air temperatures by up to 0.72°C due to enhanced convective heat and net radiation, as found by [17] in cities like Kolkata, Sydney, Austin, Athens, and Brussels. Despite climatic differences, the surface cooling-air warming trade-off remains consistent. This generalizability supports the relevance of our findings and emphasizes the need for

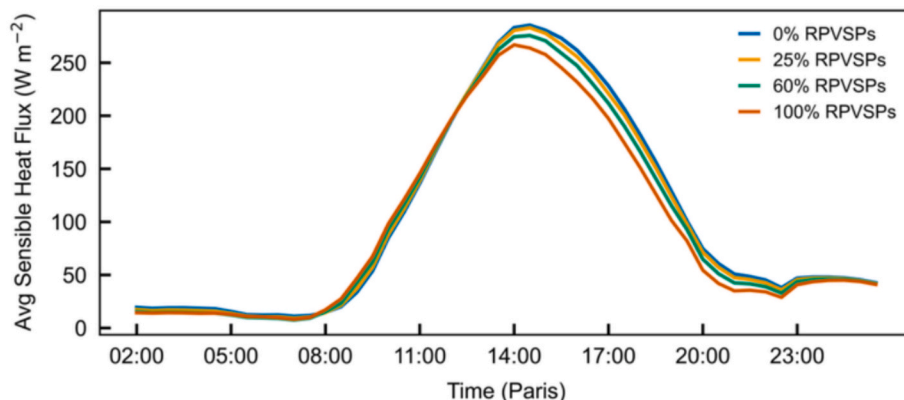


Fig. 11. Comparison of average sensible heat flux across 0 %, 25 %, 60 %, and 100 % RPVSPs deployments.

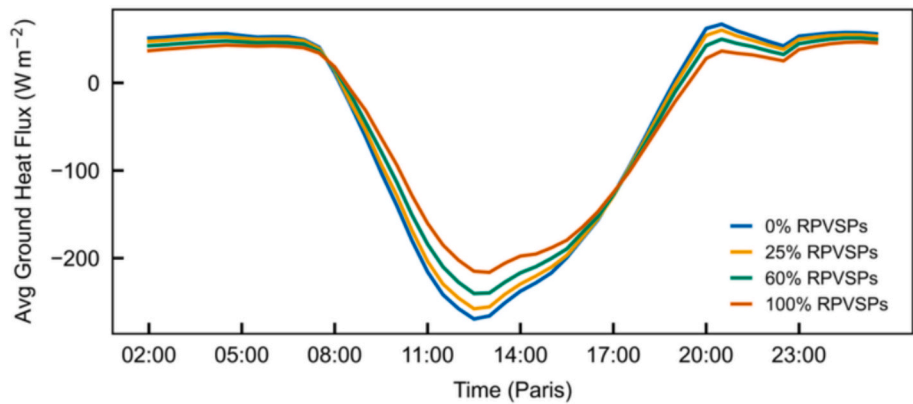


Fig. 12. Comparison of average roof heat flux across 0 %, 25 %, 60 %, and 100 % RPVSPs deployments.

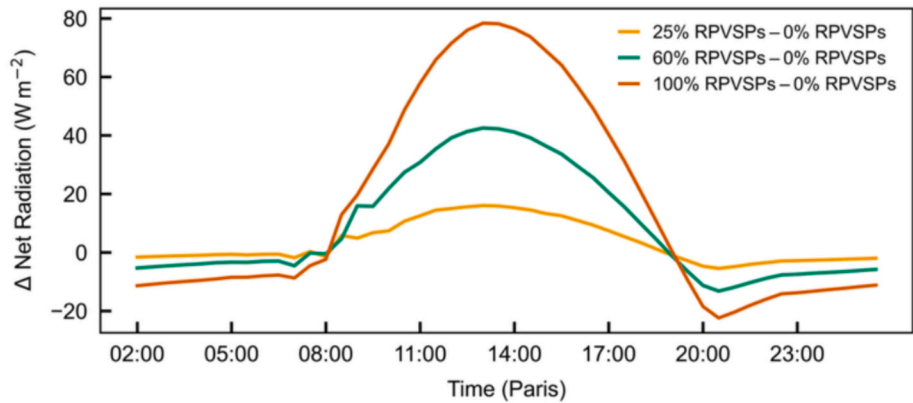


Fig. 13. Average net radiation difference for 25 %, 60 %, and 100 % RPVSPs scenarios compared to the base case (0 % RPVSPs).

integrated designs combining RPVSPs with high-albedo or vegetative strategies in various urban contexts. Our results can be extrapolated to other temperate-oceanic cities with similar built-form characteristics. Fig. 14 shows results from studies in diverse climatic contexts, including subtropical, tropical, Mediterranean, maritime, and temperate oceanic

regions, using observation and simulation methodologies to highlight the universality of these mechanisms across various climate regimes. The effects of RPVSPs on near-surface temperatures exhibit significant regional variations and diurnal fluctuations across diverse climatic contexts. In Sydney, Australia, studies have reported daytime cooling of

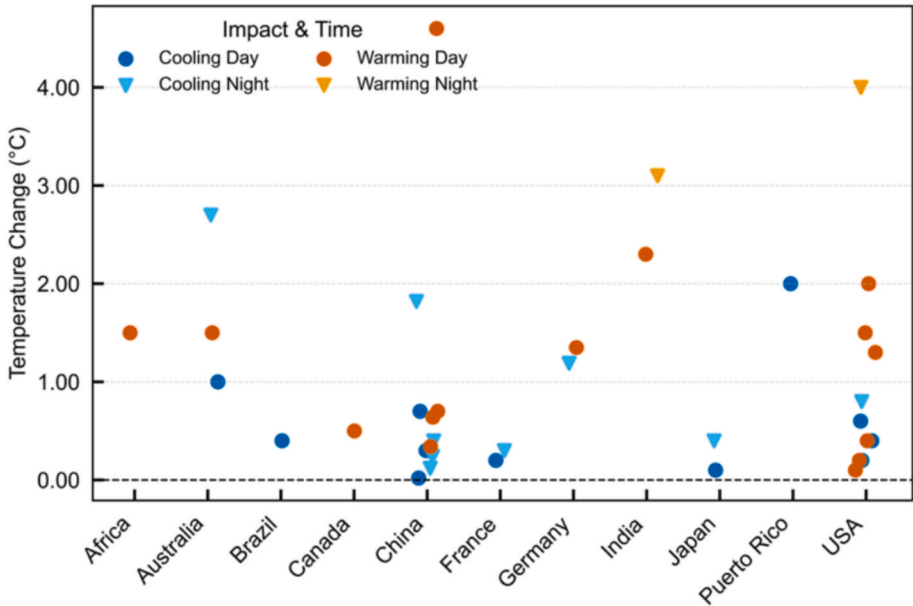


Fig. 14. RPVSPs impacts on near-surface air temperature across countries.

1.0 °C and nighttime cooling of 2.7 °C, along with a daytime warming effect of 1.5 °C [18,42]. Similarly, in Vicosa, Brazil, a moderate daytime cooling of 0.4 °C has been documented [43], while Paris, France, records reductions of 0.2 °C during the day and 0.3 °C at night [8]. In contrast, Ontario, Canada, shows a small daytime warming of 0.5 °C [44]. Osaka, Japan, exhibits limited cooling, with reductions of 0.1 °C during the day and 0.4 °C at night [45]. Across China, including Chaoyang, Gonghe, Guangzhou, Lhasa, and Qinghai Province, mixed responses are evident, with reported daytime cooling of about 0.34 °C, nighttime cooling of 0.64 °C, and daytime warming up to 1.57 °C [10,13,46–49]. In Munich, Germany, notable nighttime cooling of 1.19 °C contrasts with daytime warming of 1.35 °C [50]. A strong warming effect is observed in Pune, India, where daytime and nighttime temperatures rise by 2.3 °C and 3.1 °C, respectively [51]. In the United States, including regions such as Arizona, California, Chicago, Los Angeles, and Phoenix, mean estimates reveal daytime cooling of 0.4 °C, daytime warming of 0.92 °C, and pronounced nighttime warming approaching 4.0 °C [6,7,12,15,37,52–55]. These findings highlight the heterogeneous thermal impacts of RPVSPs, shaped by local climatic conditions, urban form, and surface-atmosphere interactions.

3.5. Air conditioning energy demand

The integration of RPVSPs systems into urban environments significantly impacts building energy dynamics, particularly affecting AC energy consumption and roof temperature variations. As RPVSPs coverage increases, there is a noticeable reduction in daytime AC energy demand, highlighting the potential of these systems to mitigate cooling loads during peak solar hours.

At 0 % RPVSPs coverage, the average AC energy consumption is 6.6 Whm⁻², with a range from 2.4 Whm⁻² to 11.2 Whm⁻², resulting in a total daytime energy demand of 213.6 Whm⁻². As coverage rises, energy consumption decreases. At 25 % RPVSPs coverage, the average AC consumption drops to 6.5 Whm⁻², further declining to 6.4 Whm⁻² at 60 % coverage and 6.3 Whm⁻² at full (100 %) RPVSPs coverage. This reduction is primarily due to the shading effect of RPVSPs, which decrease solar heat gain on building surfaces and, consequently, indoor cooling requirements. The total daytime energy demand also decreases with increasing RPVSPs coverage, from 213.6 Whm⁻² at 0 % to 210.9 Whm⁻² at 25 %, 206.9 Whm⁻² at 60 %, and 200.7 Whm⁻² at 100 %. These findings emphasize the effectiveness of RPVSPs systems in reducing cooling loads, especially during the most demanding part of the day. Although nighttime AC consumption slightly increases, from 64.2 Whm⁻² at 0 % to 64.6 Whm⁻² at 100 %, this variation is negligible compared to the substantial daytime savings. This slight increase in nighttime demand is due to the reduced ability of RPVSPs to facilitate radiative cooling from the roof at night.

Roof temperature patterns highlight the passive cooling benefits of

RPVSPs systems functioning as sunshades, as illustrated in Fig. 15. With 100 % RPVSPs coverage, the average roof temperature decreases by 1.7 °C compared to the absence of these systems. At 60 % coverage, the reduction is 1.0 °C, and at 25 % coverage, it is 0.4 °C. This temperature reduction is mainly due to the shading effect of RPVSPs, which block direct solar radiation. The cooling effect is most significant during the day, with maximum temperature reductions of −6.4 °C at 100 % RPVSPs, −3.4 °C at 60 % RPVSPs, and −1.3 °C at 25 % RPVSPs. However, while RPVSPs notably lower roof temperatures during the day, they slightly hinder the roof's ability to radiate heat at night, leading to nighttime warming effects. These include maximum temperature increases of 1.2 °C at 100 % RPVSPs, 0.7 °C at 60 % RPVSPs, and 0.3 °C at 25 % RPVSPs. Although these nocturnal warming effects may slightly increase nighttime building cooling demand, they are largely offset by the significant reductions in daytime energy demand and roof temperatures.

As shown in Fig. 16 and Table S2, previous WRF based studies consistently report reductions in building energy demand of 11 % to 14 % on the day following the deployment of RPVSPs systems [11,8,37,13,12,38]. RPVSPs mitigate roof surface heating through two synergistic processes: firstly, by providing shade that obstructs solar radiation, significantly reducing the shortwave radiation flux to the roof membrane; secondly, by enhancing convective and radiative dissipation through the ventilated air gap between the RPVSPs module and the roof. This air layer facilitates upward heat transport via natural convection and longwave infrared emission, preventing heat accumulation at the roof interface. Consequently, the roof surface under RPVSPs remains cooler during peak daytime hours, reducing conductive heat gain into the building envelope and lowering the sensible cooling load. These mechanisms result in a measurable reduction in building-level cooling energy demand, which in our simulations was approximately 4.8–5.0 % during summer daytime periods in Lyon, France. This lower reduction is due to the simultaneous increase in near-surface air temperature caused by RPVSPs, which partially offsets the expected cooling savings. The intensified surface heating from large-scale RPVSPs installations leads to higher ambient temperatures around buildings, diminishing the net energy benefit. These findings highlight the complex interplay between rooftop modifications and urban thermal dynamics, emphasizing the importance of considering both direct and indirect impacts when evaluating the synergistic benefits of RPVSPs deployment.

4. Energy generation and utilization efficiency of rooftop photovoltaic solar panels

The results indicate a significant, nearly linear increase in RPVSPs output with expanded coverage, highlighting the technology's scalability in dense urban areas and its potential to support local energy self-reliance. During solar hours (06:00–20:00 LT), the average RPVSPs yield

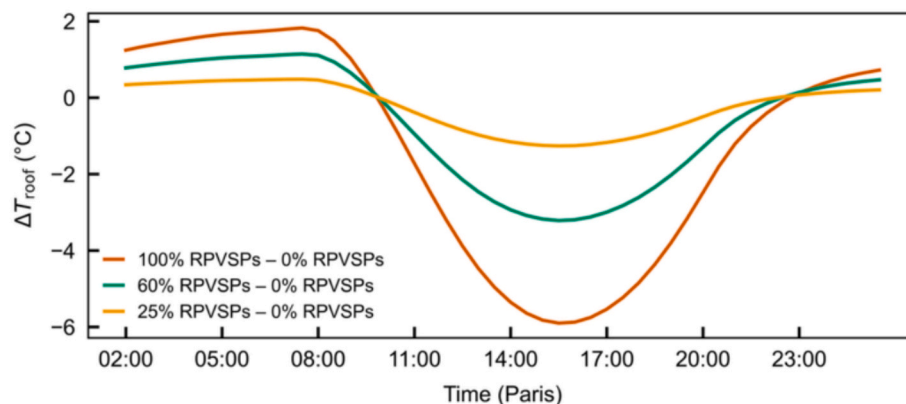


Fig. 15. Roof surface temperature differences for 25 %, 60 %, and 100 % RPVSPs coverage scenarios compared to the base case (0 % RPVSPs).

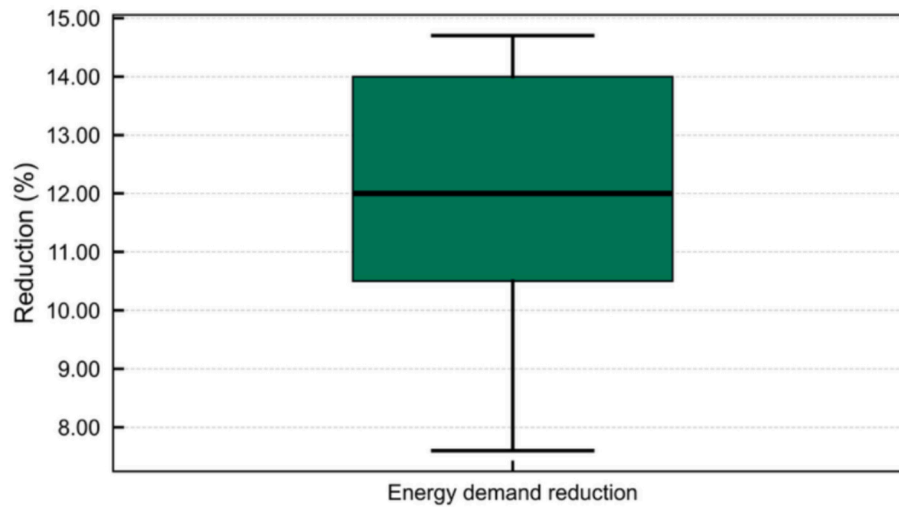


Fig. 16. Boxplot showing reported reductions (%) in building energy demand due to RPVSPs installations across various studies. The results highlight variability linked to climate, RPVSPs design, and urban characteristics.

increases from 1.3 Wh m^{-2} at 25 % coverage to 3.2 Wh m^{-2} at 60 % and 5.4 Wh m^{-2} at 100 %, as illustrated in Fig. 17. Corresponding sub-daily peaks reach 3.5, 8.5, and 14.3 Wh m^{-2} , respectively. Total daytime production follows a similar pattern, rising from 56.4 Wh m^{-2} at 25 % to 135.9 Wh m^{-2} at 60 % and 227.7 Wh m^{-2} at 100 %. These findings emphasize not only the substantial increase in energy generation but also its alignment with daytime cooling needs, which are crucial for addressing passive load imbalances in climate-sensitive regions.

The system's ability to utilize generated RPVSPs energy also improves with coverage. At 25 % RPVSPs penetration, all generated energy is consumed instantly on-site, effectively offsetting 26.8 % of the daytime AC demand. At 60 % RPVSPs, immediate utilization decreases slightly to 91.2 %, with 59.9 % of AC demand being offset. At 100 % RPVSPs, real-time utilization falls further to 64.3 %, while the AC load offset reaches its maximum of 73.0 %, as shown in Table 3. This apparent contradiction, declining real-time utilization yet rising demand, indicates a saturation point in direct consumption capacity and underscores the importance of integrating load balancing strategies.

The reduction in immediate RPVSPs utilization at higher coverage levels results from a temporal mismatch between RPVSPs generation and cooling energy demand. As RPVSPs capacity expands, particularly beyond 25 % coverage, midday generation often exceeds instantaneous AC loads. Since cooling demand typically peaks later than solar irradiance, a diurnal decoupling occurs. Without energy storage or demand-side management, this surplus generation is either curtailed or exported, reducing the on-site utilization factor. This highlights the inherent

load-generation imbalance and the critical need for integrating storage or intelligent controls to enhance operational efficiency.

4.1. Impact of energy storage systems on rooftop photovoltaic solar panels utilization and air conditioning load offset

To quantify the benefits of energy storage within different RPVSPs deployment scenarios, a battery energy storage system (BESS) model was integrated into the simulation framework. This model assesses BESS charge and discharge dynamics and their impact on RPVSPs energy utilization and AC load offset. The model calculates surplus energy $E_{ex}(t)$ and deficit energy $E_{def}(t)$ based on the RPVSPs generation $E_{RPVSPs}(t)$ and AC demand $E_{AC}(t)$ obtained from WRF simulations:

$$E_{ex}(t) = \max[0, E_{RPVSPs}(t) - E_{AC}(t)] \quad (5)$$

$$E_{def}(t) = \max[0, E_{AC}(t) - E_{RPVSPs}(t)] \quad (6)$$

The battery state-of-charge (SOC) evolves according to the following equations, which govern the energy flow within the system:

$$SOC^+(t) = \min[C_{max}, SOC(t) - E_{ch}(t)] \quad (7)$$

$$SOC(t + \Delta t) = \max[0, SOC(t) - \frac{E_{ch}(t)}{\eta}] \quad (8)$$

where $SOC(t)$ is the state-of-charge at the beginning of the timestep, $SOC^+(t)$ is the state-of-charge after charging but before discharging, and

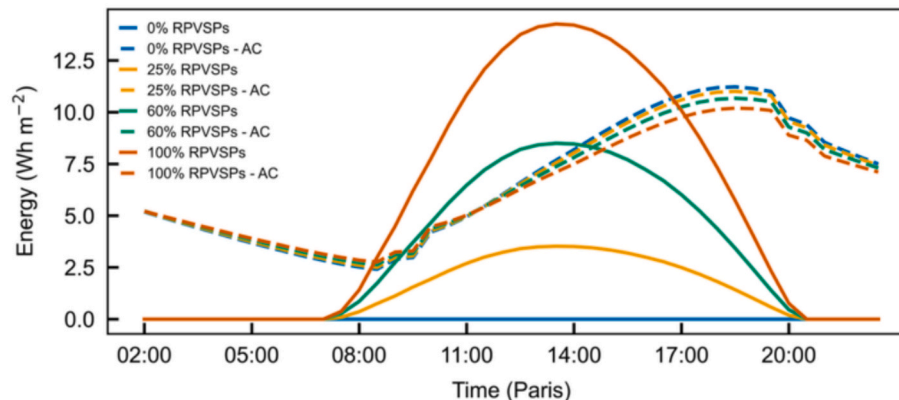


Fig. 17. RPVSPs generated energy and building AC energy consumption under 0 %, 25 %, 60 %, and 100 % RPVSPs coverage scenarios.

Table 3

RPVSPs energy utilization and AC energy offset per day.

RPVSPs coverage	Immediate RPVSPs utilization (%)	AC offset immediate (%)	RPVSPs utilization with storage (%)				AC offset with storage (%)			
			Med n = 0.7	Med n = 0.9	Lg n = 0.7	Lg n = 0.9	Med n = 0.7	Med n = 0.9	Lg n = 0.7	Lg n = 0.9
0 %	0	0	0	0	0	0	0	0	0	0
25 %	100	26.8	100	100	100	100	20.5	20.5	20.5	20.5
60 %	91.2	59.9	97.4	99.1	97.4	99.1	48.7	49.6	48.7	49.6
100 %	64.3	73.0	79.7	84.1	89.3	94.7	68.5	72.2	76.7	81.3

Δt represents timestep. The charge $E_{ch}(t)$ and discharge $E_{dis}(t)$ terms are defined to prevent overcharging or over-discharging, and to account for the available surplus or deficit:

$$E_{ch}(t) = \min[E_{ex}(t), C_{max} - SOC(t)] \quad (9)$$

$$E_{dis}(t) = \min[\eta SOC^+(t), E_{dis}(t)] \quad (10)$$

This approach ensures symmetrical application of charging and discharging losses through round-trip efficiency (η). A sensitivity analysis was conducted using two storage capacities (C_{max}): a medium capacity of 50 Whm^{-2} and a large capacity of 100 Whm^{-2} , representing the maximum energy storable per unit area within the urban domain. The round-trip efficiency (η) was evaluated at 70 % and 90 %, typical ranges for various battery chemistries and operational conditions. This led to testing four battery configurations for each RPVSPs coverage level. The integration of BESS significantly enhanced RPVSPs utilization and AC load offset, especially at higher RPVSPs penetration levels where the load-generation mismatch limits immediate consumption. The photovoltaic-self-consumption metric and cooling-load offset used in this study are defined as

$$U = \frac{E_{imm} + E_{dis}}{E_{RPVSPs}} \times 100 \quad (11)$$

$$O = \frac{E_{imm} + E_{dis}}{E_{ac}} \times 100 \quad (12)$$

where E_{imm} represents the instantaneous electricity consumption of the building, E_{dis} denotes the battery discharge over the time step, E_{RPVSPs} signifies the total RPVSPs generation, and E_{ac} indicates the air-conditioning demand. Thus, U measures the fraction of on-site solar production that is self-consumed either immediately or after storage, while O quantifies the percentage of the cooling load met by the RPVSPs and battery supply.

At 0 % and 25 % RPVSPs coverage, the BESS was inactive. With no RPVSPs at 0 % coverage, and at 25 % coverage, all 56.4 Whm^{-2} of RPVSPs output was instantaneously consumed, leaving no surplus to charge any battery configuration. This confirms that at low RPVSPs penetration levels, the entire RPVSPs output is efficiently absorbed directly by the on-site load. A substantial shift in storage utility emerged at 60 % RPVSPs coverage. The total energy generated by RPVSPs was 135.9 Whm^{-2} , with immediate RPVSPs utilization at 91.2 %, creating a daily surplus. Both medium and large BESS capacities charged an identical 11.9 Whm^{-2} , indicating that the available surplus was fully captured by the medium battery, rendering the larger capacity non-beneficial for additional charging. Discharged energy varied with efficiency, 8.4 Whm^{-2} at $\eta = 0.70$, and 10.8 Whm^{-2} at $\eta = 0.90$ as shown in the Fig. 18. This led to a notable increase in total RPVSPs utilization, rising from 91.2 % immediately to a range of 97.4–99.1 % with storage. Similarly, the AC load offset improved from 45.7 % immediately to 48.7–49.6 %.

At 100 % RPVSPs, daily generation reached 227.7 Whm^{-2} , of which only 64.3 % was immediately utilized, leaving an 81.2 Whm^{-2} surplus. A medium BESS captured 62 % of this excess and delivered 35.0 Whm^{-2} at $\eta = 0.70$ or 45.0 Whm^{-2} at $\eta = 0.90$, increasing total RPVSPs utilization

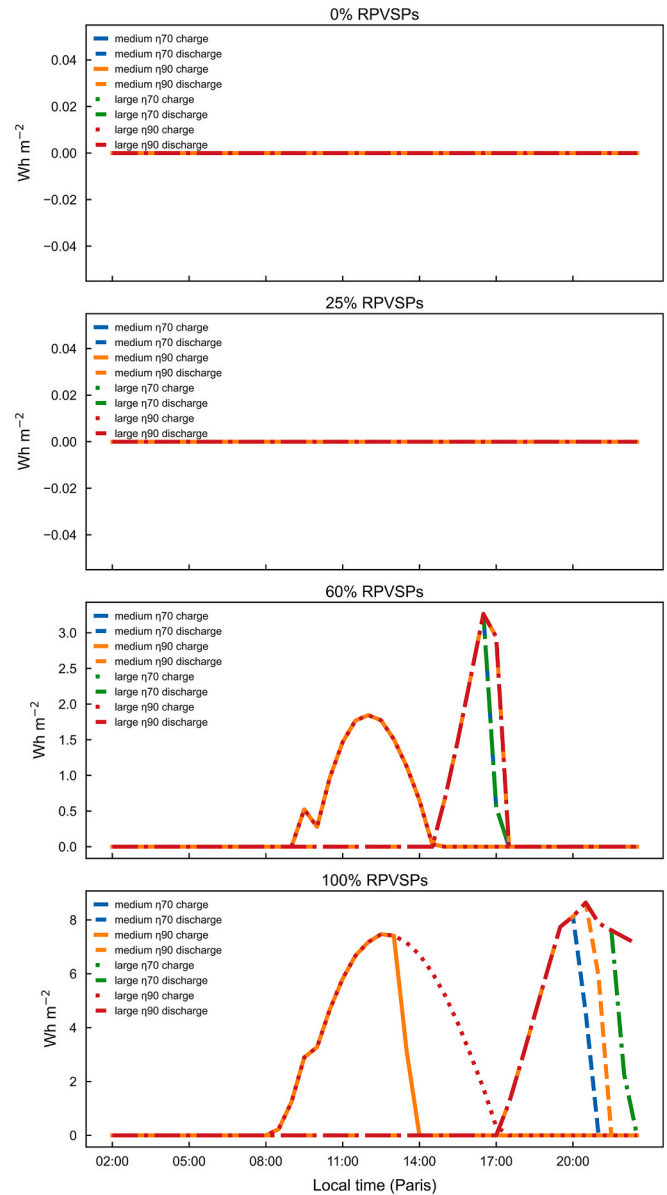


Fig. 18. Domain-averaged battery charge and discharge for RPVSPs coverages of 0 %, 25 %, 60 %, 100 %.

to 79.7–84.1 % and the AC load offset to 68.5–72.2 %. A large BESS stored the full surplus, discharging 56.8 Whm^{-2} at $\eta = 0.70$ to 69.1 Whm^{-2} at $\eta = 0.90$, elevating utilization and offset to 89.3–94.7 % and 76.7–81.3 %, respectively, as shown in the Fig. 18. Detailed numerical results for each scenario are presented in Table 3. Increasing η from 0.70 to 0.90 in the large battery yielded an additional 16 % of usable energy, underscoring the necessity of sizing storage to the daily surplus and

prioritizing high round-trip efficiency at high RPVSPs penetration. The precise battery sizing and operational strategy would depend on building-specific load profiles, diurnal irradiance variability, and prevailing tariff structures. Nevertheless, this conceptual integration underscores how storage can optimize the benefits of renewable power systems. These results highlight the efficiency and scalability of urban RPVSPs systems in meeting electricity demands during peak solar periods and their strategic value when integrated with storage solutions.

5. Sensitivity analysis of rooftop photovoltaic solar panels coverage and storage

To explore the factors influencing the decline in immediate utilization at higher RPVSPs coverage levels, a sensitivity analysis was conducted, evaluating various building topologies: compact high-rise, compact mid-rise, compact low-rise, open high-rise, open mid-rise, and open low-rise structures. At 0 % RPVSPs coverage, the average AC energy demand varied significantly, ranging from 2.8 Whm⁻² in open low-rise buildings to 24.8 Whm⁻² in compact high-rise structures, with no RPVSPs generation or storage utilization at this baseline.

At 25 % RPVSPs coverage, high demand building types such as compact and open high-rise have total AC utilization of buildings maintained 100 % immediate utilization, offsetting their AC loads by 4.9 % and 5.4 %, respectively, indicating that their high internal demand fully absorbed the generated RPVSPs as shown in Table 4 and Fig. S5. In contrast, low-demand types exhibited slightly reduced immediate utilization rates, such as 99.3 % in compact low-rise and 95.9 % in open low-rise buildings, with a small surplus of RPVSPs generation beginning to emerge. Compact low-rise charged 0.5 Whm⁻² and open low-rise charged 1.6 Whm⁻² into BESS. Storage utilization for these low-demand types, even with medium and large (70 % and 90 % round-trip efficiency) battery configurations, remained relatively low, at 1.1–1.3 % for compact low-rise and 7.0–7.8 % for open low-rise, as the surplus generation was modest. However, the overall RPVSPs utilization in low-demand urban typologies experienced a slight improvement with storage, reaching 99.9 % for compact low-rise and 99.6 % for open low-rise. This marginal increase in utilization resulted in higher total AC load offset values of 26.4 % and 29.4 %, respectively, under the 25 % RPVSPs scenario as shown in Fig. S6.

At 60 % RPVSPs coverage, high-demand building types maintained 100 % immediate utilization due to their consistently high energy loads, achieving AC offsets of 11.9 % for compact high-rise and 13.0 % for open high-rise. In contrast, lower-demand types experienced significant declines in immediate utilization. Compact mid-rise utilization fell to 96.3 %, with 7.8 Whm⁻² charged into BESS as shown in Table and Fig. S7. With battery storage, overall RPVSPs utilization increased to 99.6 %, and the AC offset rose from 37.4 % to 38.7 %. Compact low-rise utilization dropped sharply to 69.2 %, indicating substantial surplus generation, with 59.6 Whm⁻² charged into large storage and 50.0 Whm⁻² into medium storage. BESS integration improved total RPVSPs utilization to 96.9 %, increasing the AC offset from 44.7 % to 62.6 % with large storage at 90 % round-trip efficiency. Similarly, open mid-rise utilization decreased to 95.1 %, with 5.5 Whm⁻² charged, and overall RPVSPs utilization rose to 99.5 %, increasing the AC offset from 37.3 % to 39.0 %. Open low-rise utilization also declined significantly to 64.7 %, with 33.5 Whm⁻² charged into storage. Battery integration for open low-rise buildings boosted total RPVSPs utilization to 96.5 % and increased the AC offset from 47.1 % to 70.3 % with medium and large storage at 90 % round-trip efficiency as shown in Fig. S8. The increased charged and discharged values for medium and low-rise types at this coverage highlight the growing role of storage in managing surplus generation.

At 100 % RPVSPs deployment, compact and open high-rise buildings still achieved 100 % immediate utilization, significantly offsetting AC demands by up to 20.1 % and 21.9 %, respectively, with no recorded battery charging or discharging, reinforcing their consistent high demand. However, mid-rise and low-rise types showed pronounced

Table 4

Total RPVSPS generation, AC energy demand, and corresponding immediate utilization and offset rates across six urban typologies under four RPVSPs deployment scenarios (0 %, 25 %, 60 %, and 100 %). Immediate RPVSPS utilization represents the percentage of RPVSPS energy consumed on-site without storage, while AC offset reflects the proportion of total cooling demand met directly by RPVSPS generation.

RPVSPs coverage (%)	Urban type	Total RPVSPs (Wh m ⁻²)	Total AC (Wh m ⁻²)	RPVSPs util immediate (%)	AC off immediate (%)
0	Compact high rise	0	1188.8	0	0
	Compact mid rise	0	545.5	0	0
	Compact low rise	0	306.6	0	0
	Open high rise	0	638.4	0	0
	Open mid rise	0	288.6	0	0
	Open low rise	0	134.9	0	0
25	Compact high rise	58.2	1183	100	4.9
	Compact mid rise	86.5	541.8	100	16
	Compact low rise	80.4	304.1	99.3	26.3
	Open high rise	34.1	636.1	100	5.4
	Open mid rise	46.0	286.5	100	16.1
	Open low rise	39.3	133.1	95.9	28.3
60	Compact high rise	140.2	1179.3	100	11.9
	Compact mid rise	208.4	535.9	96.3	37.4
	Compact low rise	193.8	299.9	69.2	44.7
	Open high rise	82.2	633.0	100	13.0
	Open mid rise	110.9	282.9	95.1	37.3
	Open low rise	94.9	130.1	64.7	47.1
100	Compact high rise	234.8	1168.3	100	20.1
	Compact mid rise	349.0	525.5	69.9	46.4
	Compact low rise	324.4	291.3	45.7	50.8
	Open high rise	137.7	628.3	100	21.9
	Open mid rise	185.7	277.0	69.8	46.8
	Open low rise	158.8	125.5	41.8	52.9

decreases in immediate utilization, dropping to 69.9 % for compact mid-rise, 45.7 % for compact low-rise, 69.8 % for open mid-rise, and 41.8 % for open low-rise buildings as shown in Fig. 19 and Table 4. This was attributed to substantial RPVSPs generation surpassing immediate internal demand during peak irradiance periods. The integration of BESS at 100 % RPVSPs coverage significantly mitigated the impact of surplus generation on overall RPVSPs utilization and AC offset for these building typologies. For compact mid-rise buildings, RPVSPs utilization improved to 95.7 % with storage, and AC offset increased from 46.4 % to 63.6 % with large storage at 90 % round-trip efficiency charging 100.0 Whm⁻². Compact low-rise buildings saw RPVSPs utilization rise to 73.4

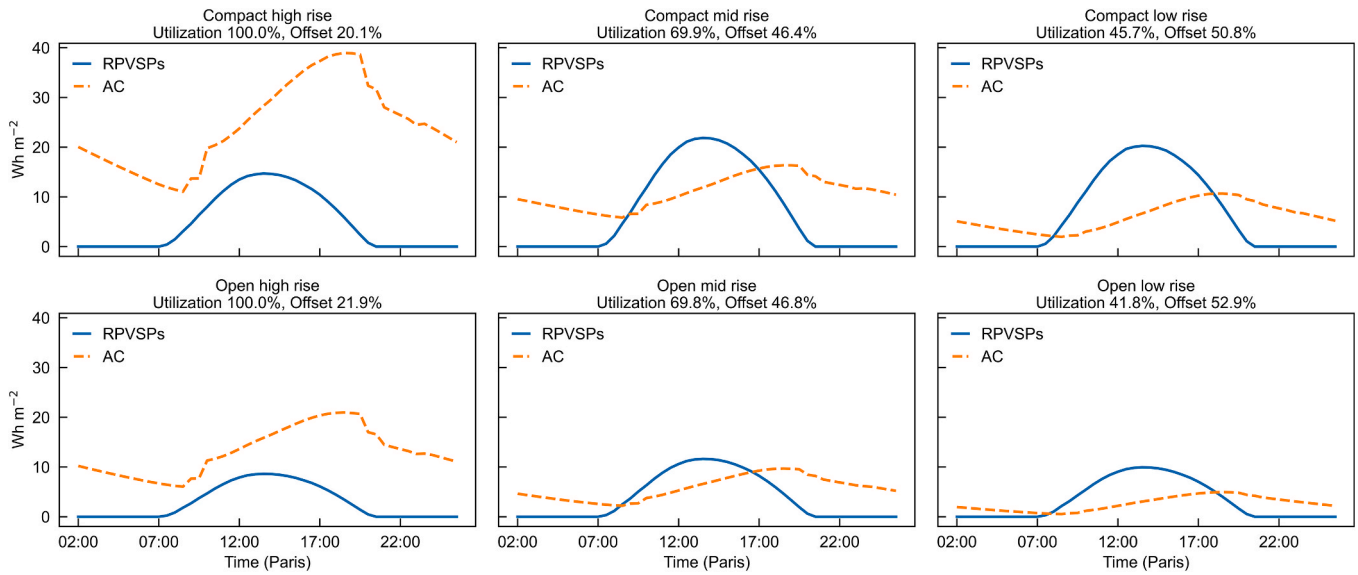


Fig. 19. Diurnal profiles of RPVSPs generation and AC cooling demand (Wh m^{-2}) for six urban building types under 100 % RPVSPs coverage.

% with large storage at 90 % round-trip efficiency, achieving an 81.7 % AC offset from 50.8 %, with 100.0 Wh m^{-2} charged. Open mid-rise buildings achieved 97.0 % RPVSPs utilization with large storage at 90 % round-trip efficiency, improving AC offset from 46.8 % to 65.0 %, with 56.0 Wh m^{-2} charged. Open low-rise buildings, charging 92.4 Wh m^{-2} into large storage, reached 69.7 % RPVSPs utilization and an impressive 88.2 % AC offset from 52.9 % as shown in Fig. 20. The utilization metric for BESS, especially at 100 % coverage and with large storage sizes, shows a significant increase of 58.6 % for compact low-rise and 86.1 % for open low-rise, indicating effective utilization of stored energy to meet demand when RPVSPs generation is low.

The primary factor influencing these patterns is closely linked to building morphology, particularly the roof-to-volume ratio. High-rise buildings, with smaller roof areas relative to their large internal

volumes, limit the maximum feasible RPVSPs integration, maintaining high immediate utilization rates and minimal storage needs. In contrast, mid-rise and low-rise buildings, with larger roof areas compared to their internal volumes, allow for greater RPVSPs installations, often resulting in surplus generation beyond immediate demand. The sensitivity analysis with BESS shows that for these building types, energy storage is crucial for enhancing overall RPVSPs utilization efficiencies by capturing and later discharging surplus energy, significantly increasing the total AC offset.

This extended sensitivity analysis illustrates the dynamic relationship between building morphology, RPVSPs coverage, and energy utilization efficiency, further supporting the mechanisms behind the decline in immediate utilization at higher RPVSPs deployments and emphasizing the need for optimized sizing and integration of energy

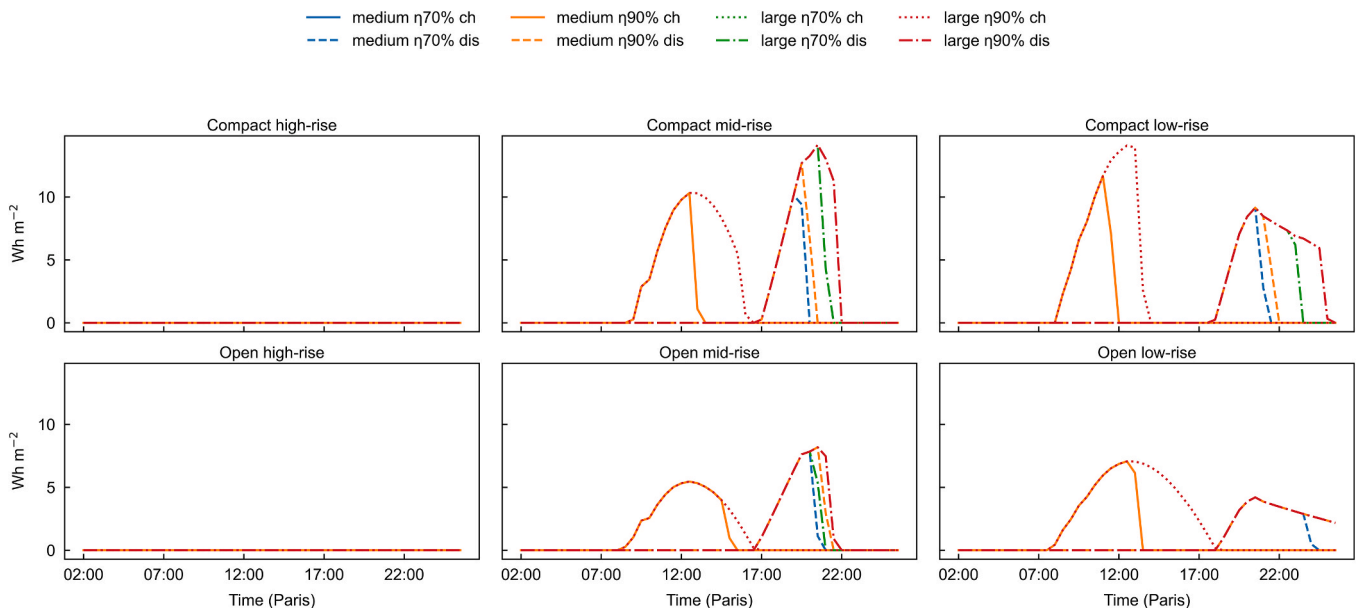


Fig. 20. Charging and discharging patterns (Wh m^{-2}) of medium and large BESS at 70 % and 90 % round-trip efficiencies across six urban typologies under 100 % RPVSPs deployment. Compact and open high-rise buildings exhibit no storage activity due to their high AC loads fully absorbing generated RPVSPs energy. In contrast, mid- and low-rise buildings, particularly compact mid-rise and open low-rise, demonstrate substantial battery charging during midday and discharging in the evening, indicating a pronounced temporal mismatch between generation and demand. Peak discharging exceeds 10 Wh m^{-2} in high-efficiency configurations, significantly enhancing RPVSPs utilization.

storage to manage energy surplus and maximize the benefits of RPVSPs in urban energy systems. The insights gained underscore the importance of customized RPVSPs sizing strategies and integrated storage solutions for optimizing urban energy systems, particularly for building types with high RPVSPs generation potential relative to their immediate demand.

6. Trade-offs between cooling and warming effects

RPVSPs installations exert dualistic impacts on urban thermal dynamics emphasizing the inherent trade-offs between their cooling benefits and localized warming effects. Quantitatively, at peak solar noon (12:00 LT), the implementation of 100 % RPVSPs coverage significantly reduces the downward conductive heat flux into buildings from -257.70 W m^{-2} (baseline) to -202.38 W m^{-2} , corresponding to a net decrease of approximately 55.3 W m^{-2} . This diminished conductive heat load directly translates to a reduction in roof-surface temperature by $\sim 1.7^\circ\text{C}$, which subsequently lowers building cooling demand, evidenced by an estimated 5 % decrease AC energy consumption. This outcome underscores the effective thermal barrier function of RPVSPs panels, mitigating heat gain by shading and altered surface energy partitioning. Conversely, the presence of RPVSPs arrays modifies the surface energy balance by increasing the sensible heat flux from 112.3 W m^{-2} at 25 % RPVSPs coverage to 121.1 W m^{-2} at full coverage. This increase in turbulent heat flux, coupled with an augmentation in net daytime radiation by up to $+76.5 \text{ W m}^{-2}$, contributes to localized ambient air temperature elevations of up to $+0.72^\circ\text{C}$, as demonstrated in Figs. 12, 14, and 15. These warming effects are attributable to changes in surface albedo and thermal emissivity induced by RPVSPs materials, which absorb more solar radiation than high-albedo roofing alternatives and re-emit heat into the urban canopy layer. Further, we investigate nocturnal dynamics, revealing that RPVSPs can hinder radiative cooling at night, increasing roof surface temperatures by up to $+1.2^\circ\text{C}$ compared to conventional roofing. This occurs because RPVSPs modules reduce the effective longwave emissivity of the roof and obstruct sky view factors, thereby suppressing radiative heat loss. However, RPVSPs simultaneously emit elevated longwave radiation relative to traditional roofing materials, partially offsetting this effect. Comparative analysis with passive heat mitigation strategies such as cool roofs and green roofs shows that these interventions typically yield consistent reductions in both roof and ambient air temperatures of $1\text{--}2^\circ\text{C}$, without electricity generation. Their higher albedo and evapotranspiration processes improve urban heat stress with minimal localized warming trade-offs. Based on these findings, we propose that hybrid approaches, integrating RPVSPs with reflective coatings or vegetative layers, may optimize the trade-offs between electricity generation and urban heat mitigation. Such synergistic strategies can simultaneously leverage the renewable energy benefits of RPVSPs installations while preserving or enhancing urban cooling effects, thereby aligning with sustainable urban climate resilience goals.

7. Limitations of the study

While this study provides valuable insights into the thermal and energy performance of RPVSPs, several limitations must be acknowledged to contextualize its findings. The simulations were conducted under idealized conditions, assuming uniform RPVSPs coverage and tailored to the specific climatic, architectural, and urban morphology characteristics of Lyon, France. Although this ensured internal consistency, it limits the generalizability of the results to cities with different climatic conditions, solar radiation patterns, urban configurations, or building typologies. For instance, cities in arid, tropical, or extremely cold climates may exhibit distinct interactions between RPVSPs installations and the urban thermal environment due to differences in atmospheric dynamics and energy fluxes. Furthermore, the model assumed homogeneous RPVSPs system deployment with ideal

operational parameters. Installations are highly heterogeneous, varying in panel coverage, module efficiency, orientation, tilt angles, cleaning practices, and degradation rates. These factors can substantially affect both energy generation and thermal performance. While simplifying assumptions were necessary for model tractability, incorporating these operational complexities would improve the representativeness of results in applied settings. The simulations did not capture interactions between RPVSPs and surrounding urban surfaces such as façades, adjacent buildings, roads, and vegetated areas. Secondary radiation exchanges, inter-surface shading, and alterations to pedestrian-level microclimates were not explicitly modeled. These factors are particularly relevant in dense urban environments, where thermal feedback between surfaces may significantly influence outcomes.

In addition, the study neglected to consider dynamic atmospheric variability, such as interannual weather fluctuations, extreme heat events, and long-term climate change projections. These temporal factors can significantly influence system performance and urban thermal responses, and their exclusion restricts the assessment of resilience or adaptation potential under changing climatic conditions. Future research should address these limitations by incorporating spatial and operational heterogeneity, urban surface interactions, and dynamic climate scenarios to enhance the robustness and applicability of simulation-based evaluations of RPVSPs in various urban settings.

8. Conclusion

This study evaluates the thermal and energy implications of RPVSPs within the urban setting of Lyon, France, with a primary focus on their influence on near-surface air temperatures, building energy consumption, and energy production. The findings reveal a dual thermal effect: while RPVSPs effectively convert incident solar energy into electricity, they also induce localized daytime warming, resulting in an increase of up to 0.72°C in near-surface air temperatures under 100 % coverage. This warming is attributed to the panels' enhanced solar absorption, elevated surface temperatures, and intensified convective heat transfer with the surrounding air. Conversely, nighttime conditions exhibit a net cooling effect, with air temperatures reduced by up to 0.42°C relative to scenarios without RPVSPs. In terms of building performance, RPVSPs reduce daytime roof surface temperatures by an average of 2.09°C at full coverage leading to a nearly 5 % reduction in daytime AC energy demand. However, diminished nighttime radiative cooling results in a slight elevation of roof temperatures by 1.61°C , marginally increasing nighttime cooling loads. Notably, energy generation from RPVSPs plays a pivotal role in offsetting electricity consumption. At 100 % coverage, the panels produced an average of 227.7 Whm^{-2} , effectively offsetting 85.9 % of the total daily AC energy demand of 265.1 Whm^{-2} . These findings underscore the strategic significance of RPVSPs as an integrated solution for urban energy systems providing clean energy generation and reductions in cooling demand. Nevertheless, the potential for daytime heating effects underscores the necessity of context-specific planning and thermal impact assessment. Future research should expand upon this work by exploring diverse RPVSPs layouts, incorporating more detailed urban morphologies, and assessing system performance under future climate scenarios. Furthermore, hybrid configurations that combine RPVSPs with reflective or vegetated roofing materials may offer a promising avenue to maximize energy efficiency while mitigating unintended thermal consequences in densely populated urban environments.

CRedit authorship contribution statement

Hamza Nisar: Writing – original draft, Visualization, Validation, Software, Methodology, Formal analysis. **Mattheos Santamouris:** Writing – review & editing, Supervision, Project administration, Funding acquisition. **Christophe Menezo:** Writing – review & editing, Supervision, Project administration, Funding acquisition. **Ansar Khan:**

Writing – review & editing, Investigation, Conceptualization.

Declaration of competing interest

The authors declare that they have no known competing financial interests or personal relationships that could have appeared to influence the work reported in this paper.

Acknowledgments

Co-funded by the European Union under the Marie Skłodowska-Curie Grant Agreement No. 101081465 (AUFRADE). Views and opinions expressed are however those of the authors only and do not necessarily reflect those of the European Union or the Research Executive Agency. Neither the European Union nor the Research Executive Agency can be held responsible for them.

Appendix A. Supplementary data

Supplementary data to this article can be found online at <https://doi.org/10.1016/j.solener.2025.113928>.

References

- [1] C. Efthymiou, A. Khan, M.N. Assimakopoulos, M. Santamouris, Urban pavement-mounted photovoltaics as renewable energy systems for energy generation and microclimate control, *Solar Energy* 299 (2025) 113780.
- [2] S. Garshabi, A. Khan, M. Santamouris, On the building cooling energy penalty of photovoltaic solar panels in Sydney, *Energy Build* 294 (2023) 113259.
- [3] S. Khorat, R. Khatun, D. Das, A. Siddiqui, A. Khan, N. Mondal, S.M. Aziz, P. Anand, Q. Van Doan, D. Niyogi, M. Santamouris, Quantifying outdoor heat stress potential due to city-wide installation of rooftop photovoltaic solar panels, *Energy and Buildings* (2025) 115996.
- [4] K. Vasilakopoulou, G. Ulpiani, A. Khan, A. Synnefa, M. Santamouris, Cool roofs boost the energy production of photovoltaics: Investigating the impact of roof albedo on the energy performance of monofacial and bifacial photovoltaic modules, *Solar Energy* 265 (2023) 111948.
- [5] D. Sailor, J. Anand, R. King, Photovoltaics in the built environment: a critical review, *Energy. Buildings* 253 (2021) 111479.
- [6] G.A. Barron-Gafford, R.L. Minor, N.A. Allen, A.D. Cronin, A.E. Brooks, M.A. Pavao-Zuckerman, The photovoltaic heat island effect: larger solar power plants increase local temperatures, *Sci. Rep.* 6 (1) (2016) 35070.
- [7] H. Taha, The potential for air-temperature impact from large-scale deployment of solar photovoltaic arrays in urban areas, *Sol. Energy* 91 (2013) 358–367.
- [8] V. Masson, M. Bonhomme, J.-L. Salagnac, X. Briottet, A. Lemonsu, Solar panels reduce both global warming and urban heat island, *Front. Environ. Sci.* 2 (2014) 14.
- [9] O. Brousse, C. Simpson, A. Zonato, A. Martilli, J. Taylor, M. Davies, C. Heaviside, Cool roofs could be most effective at reducing outdoor urban temperatures in London (United Kingdom) compared with other roof top and vegetation interventions: a mesoscale urban climate modeling study, *Geophys. Res. Lett.* 51 (13) (2024) e2024GL109634.
- [10] B. Chen, W. Wang, Y. You, W. Zhu, Y. Dong, Y. Xu, M. Chang, X. Wang, Influence of rooftop mitigation strategies on the thermal environment in a subtropical city, *Urban Clim.* 49 (2023) 101450.
- [11] J. Chen, N. Dong, Z. Liu, Y. Chen, M. Luo, H. Huang, Local temperature impact of urban heat mitigation strategy based on wrf integrating urban canopy parameters and local climate zones, *Build. Environ.* 267 (2025) 112257.
- [12] H. Tan, R. Kotamarthi, J. Wang, Y. Qian, T. Chakraborty, Impact of different roofing mitigation strategies on near-surface temperature and energy consumption over the Chicago metropolitan area during a heatwave event, *Sci. Total Environ.* 860 (2023) 160508.
- [13] L. Shen, H. Li, L. Guo, B.-J. He, Thermal and energy benefits of rooftop photovoltaic panels in a semi-arid city during an extreme heatwave event, *Energ. Buildings* 275 (2022) 112490.
- [14] H. Zhou, W. Chen, S. Hu, F. Yang, Model simulation of thermal environment and energy effects of rooftop distributed photovoltaics, *Global Energy Interconnect.* 7 (6) (2024) 723–732.
- [15] A.M. Broadbent, E.S. Krayenhoff, M. Georgescu, D.J. Sailor, The observed effects of utility-scale photovoltaics on near-surface air temperature and energy balance, *J. Appl. Meteorol. Climatol.* 58 (5) (2019) 989–1006.
- [16] He, Y., Hui, D. J. C., and Wong, N. H. (2024). Solar photovoltaics deployment impact on urban temperature: review and assessment recommendations. *Building and Environment*, page 111920.
- [17] A. Khan, P. Anand, S. Garshabi, R. Khatun, S. Khorat, R. Hamdi, D. Niyogi, M. Santamouris, Rooftop photovoltaic solar panels warm up and cool down cities, *Nat. Cities* 1 (11) (2024) 780–790.
- [18] A. Khan, M. Santamouris, On the local warming potential of urban rooftop photovoltaic solar panels in cities, *Sci. Rep.* 13 (2023) 15623.
- [19] A. Zonato, A. Martilli, E. Gutierrez, F. Chen, C. He, M. Barlage, D. Zardi, L. Giovannini, Exploring the effects of rooftop mitigation strategies on urban temperatures and energy consumption, *J. Geophys. Res. Atmos.* 126 (21) (2021) e2021JD035002.
- [20] A. Dominguez, J. Kleissl, J.C. Luvall, Effects of solar photovoltaic panels on roof heat transfer, *Sol. Energy* 85 (9) (2011) 2244–2255.
- [21] Demuzere, M., He, C., Martilli, A., and Zonato, A. (2023). Technical documentation for the hybrid 100 m global land cover dataset with local climate zones for wrf.
- [22] F. Salamanca, A. Krpo, A. Martilli, A. Clappier, A new building energy model coupled with an urban canopy parameterization for urban climate simulations-part i. formulation, verification, and sensitivity analysis of the model, *Theor. Appl. Climatol.* 99 (3–4) (2010) 331–344.
- [23] G. Balsamo, et al., ERA-interim/land: a global land surface reanalysis data set, *Hydrol. Earth Syst. Sci.* 19 (1) (2015) 389–407.
- [24] J. Lian, et al., Evaluation of the WRF-UCM mesoscale model and ECMWF global operational forecasts over the Paris region in the prospect of tracer atmospheric transport modeling, *Elementa* 6 (2018).
- [25] S.Y. Hong, J.-O.-J. Lim, The WRF single-moment 6-class microphysics scheme (wsm6), *Asia Pac. J. Atmos. Sci.* 42 (2) (2006) 129–151.
- [26] F. Chen, J. Dudhia, Coupling an advanced land surface–hydrology model with the penn state–ncar mm5 modeling system. part i: Model implementation and sensitivity, *Mon. Weather Rev.* 129 (4) (2001) 569–585.
- [27] P. Bougeault, P. Lacarrere, Parameterization of orography-induced turbulence in a mesobeta-scale model, *Mon. Weather Rev.* (1989).
- [28] Z.I. Janjic, The step-mountain eta coordinate model: further developments of the convection, viscous sublayer, and turbulence closure schemes, *Mon. Weather Rev.* 122 (5) (1994) 927–945.
- [29] J. Dudhia, Numerical study of convection observed during the winter monsoon experiment using a mesoscale two-dimensional model, *J. Atmos. Sci.* 46 (20) (1989) 3077–3107.
- [30] E.J. Mlawer, S.J. Taubman, P.D. Brown, M.J. Iacono, S.A. Clough, Radiative transfer for inhomogeneous atmospheres: Rrtm, a validated correlated-k model for the longwave, *J. Geophys. Res. Atmos.* 102 (D14) (1997) 663–679.
- [31] J.S. Kain, The Kain–Fritsch convective parameterization: an update, *J. Appl. Meteorol.* 43 (1) (2004) 170–181.
- [32] A. Jones, C. Underwood, A thermal model for photovoltaic systems, *Sol. Energy* 70 (4) (2001) 349–359.
- [33] A. Jones, C. Underwood, A modelling method for building-integrated photovoltaic power supply, *Build. Serv. Eng. Res. Technol.* 23 (3) (2002) 167–177.
- [34] A. Scherba, D.J. Sailor, T.N. Rosenstiel, C.C. Wamser, Modeling impacts of roof reflectivity, integrated photovoltaic panels and green roof systems on sensible heat flux into the urban environment, *Build. Environ.* 46 (12) (2011) 2542–2551.
- [35] Bouyer, J., Musy, M., Huang, Y., Athamena, K. (2011). Mitigating urban heat island effect by urban design: forms and materials. *Cities and Climate Change: Responding to an Urgent Agenda*, pages 164–181.
- [36] Synnefa, A. and Santamouris, M. (2016). Mitigating the urban heat with cool materials for the buildings' fabric. In *Urban Climate Mitigation Techniques*, pages 67–91. Routledge.
- [37] F. Salamanca, M. Georgescu, A. Mahalov, M. Moustauoui, A. Martilli, Citywide impacts of cool roof and rooftop solar photovoltaic de-ployment on near-surface air temperature and cooling energy demand, *Bound.-Lay. Meteorol.* 161 (203–221) (2016) 9.
- [38] W. Zhou, X. Li, L. Duanmu, C. Yuan, Investigation on rooftop pv performance and impact on microclimate in tropical cities—a wrf modelling study in Singapore, *Renew. Energy* 237 (2024) 121675.
- [39] Y. Hirano, Y. Yoshida, Assessing the effects of co2 reduction strategies on heat islands in urban areas, *Sustain. Cities Soc.* 26 (2016) 383–392.
- [40] R. Pokhrel, A. Walker, J.E. Gonzalez, A new method-ology to assess building integrated roof top photovoltaic installations at city scales: the tropical coastal city case, *J. Eng. Sustain. Build. Cities* 1 (1) (2020) 011004.
- [41] C. Peng, J. Yang, The effect of photovoltaic panels on the rooftop temperature in the energypus simulation environment, *Int. J. Photoenergy* 2016 (1) (2016) 9020567.
- [42] S. Ma, M. Goldstein, A. Pitman, N. Haghdadi, I. MacGill, Pricing the urban cooling benefits of solar panel deployment in Sydney, Australia, *Sci. Rep.* 7 (1) (2017) 43938.
- [43] C.P. Oliveira, F.C.D. Sousa, G.M. Dallago, J.R. Silva, P.H.R.F. Campos, M.C.D. C. Guimaraes, F.D.C. Baeta, Thermal environment and animal comfort of aviary prototypes with photovoltaic solar panel on the roof, *Energies* 16 (5) (2023) 2504.
- [44] U. Berardi, J. Graham, Investigation of the impacts of microclimate on pv energy efficiency and outdoor thermal comfort, *Sustain. Cities Soc.* 62 (2020) 102402.
- [45] A. Cortes, Y. Murashita, T. Matsuo, A. Kondo, H. Shimadera, Y. Inoue, Numerical evaluation of the effect of photovoltaic cell installation on urban thermal environment, *Sustain. Cities Soc.* 19 (2015) 250–258.
- [46] R. Chang, Y. Shen, Y. Luo, B. Wang, Z. Yang, P. Guo, Observed surface radiation and temperature impacts from the large-scale deployment of photovoltaics in the barren area of Gonghe, China, *Renew. Energy* 118 (2018) 131–137.
- [47] Wu, W., Qin, Y., Yue, S., and Ren, L. (2021). Observational study on the impact of large-scale photovoltaic development on soil temperature. In *IOP Conference Series: Earth and Environmental Science*, volume 826, page 012038. IOP Publishing.
- [48] L. Yang, X. Gao, F. Lv, X. Hui, L. Ma, X. Hou, Study on the local climatic effects of large photovoltaic solar farms in desert areas, *Sol. Energy* 144 (2017) 244–253.
- [49] Y. Zhong, H. Yu, W. Wang, P. Yu, Impacts of future urbanization and rooftop photovoltaics on the surface meteorology and energy balance of Lhasa, china, *Urban Clim.* 51 (2023) 101668.

- [50] E. Fassbender, S. Pytlik, J. Rott, C. Hemmerle, Impacts of rooftop photovoltaics on the urban thermal microclimate: metrological investigations, *Buildings* 13 (9) (2023) 2339.
- [51] Mandavgane, A., Karve, S., Kulkarni, P., Dhamankar, N. (2022). The impact of solar photovoltaic (pv) rooftop panels on temperature profiles of surroundings and urban thermal environment. In *International Conference on Advances in Energy Research*, pages 409–419. Springer.
- [52] Fthenakis, V. and Yu, Y. (2013). Analysis of the potential for a heat island effect in large solar farms. In *2013 IEEE 39th photovoltaic specialists conference (PVSC)*, pages 3362–3366. IEEE.
- [53] B. Lebassi, J. Gonzalez, R. Bornstein, On the environmental sustainability of building integrated solar technologies in a coastal city, *J. Sol. Energy Eng.* 135 (4) (2013) 040904.
- [54] D. Millstein, S. Menon, Regional climate consequences of large-scale cool roof and photovoltaic array deployment, *Environ. Res. Lett.* 6 (3) (2011) 034001.
- [55] J.V. Pham, A. Baniassadi, K.E. Brown, J. Heusinger, D.J. Sailor, Comparing photovoltaic and reflective shade surfaces in the urban environment: effects on surface sensible heat flux and pedestrian thermal comfort, *Urban Clim.* 29 (2019) 100500.